Scientific Reports

https://doi.org/10.1038/s41598-026-40449-y

Article in Press

Synthesis and biological evaluation of 6-hydroxychromone based thiosemicarbazones as potential antidiabetic and antioxidant agents

Received: 5 November 2025

Accepted: 12 February 2026

Published online: 22 February 2026

Cite this article as: Zareen W., Ahmed N., Siddique F. *et al.* Synthesis and biological evaluation of 6-hydroxychromone based thiosemicarbazones as potential antidiabetic and antioxidant agents. *Sci Rep* (2026). https://doi.org/10.1038/s41598-026-40449-y

Wajeeha Zareen, Nadeem Ahmed, Farhan Siddique, Parham Taslimi, Muhammad Ali Khan, Talha Islam, Mostafa A. Ismail, Mariya al-Rashida, Magdi E. A. Zaki, Sobhi M. Gomha, Rima D. Alharthy & Zahid Shafiq

Synthesis and biological evaluation of 6-hydroxychromone based thiosemicarbazones as potential antidiabetic and antioxidant agents

Wajeeha Zareen[a], Nadeem Ahmed[a,b], Farhan Siddique[c], Parham Taslimi[d], Ali Muhammad Khan[a], Talha Islam[e], Mostafa A. Ismail[f], Mariya al-Rashida[e], Magdi E. A. Zaki[g], Sobhi M. Gomha[h]*, Rima D. Alharthy[i] and Zahid Shafiq[a]*

[a] *Institute of Chemical Sciences, Bahauddin Zakariya University, 60800, Multan, Pakistan.*
[b]*College of Chemistry & Chemical Engineering, Central South University, Changsha,*
Hunan 410083, China.
[c]*Department of Pharmaceutical Chemistry, Faculty of Pharmacy, Bahauddin Zakariya University, Multan-60800, Pakistan*
[d]*Department of Biotechnology, Faculty of Science, Bartin University, 74110 Bartin, Türkiye*
[e]*Department of Chemistry, Forman Christian College (A Chartered University), Ferozepur Road 54600, Lahore, Pakistan*
[f]*Research Center for Advanced Materials Science (RCAMS), Chemistry Department, Faculty of Science, King Khalid University, P.O. Box 960, Abha 61413, Saudi Arabia*
[g]*Department of Chemistry, Faculty of Science, Imam Mohammad Ibn Saud Islamic University (IMSIU), Riyadh 11623, Saudi Arabia*
[h]*Department of Chemistry, Faculty of Science, Islamic University of Madinah, Madinah, 42351, Saudi Arabia*
[i]*Department of Chemistry, Science & Arts College, Rabigh Branch, King Abdulaziz University, Rabigh 21911, Saudi Arabia*

Corresponding Author:

Prof. Dr. Zahid Shafiq: zahidshafiq@bzu.edu.pk
Prof. Dr. Sobhi M. Gomha: smgomha@iu.edu.sa

Abstract

A new series of 6-hydroxychromone-based thiosemicarbazones **4(a-p)** was synthesized and assessed for their antidiabetic (α-Glucosidase and α-Amylase inhibition) as well as antioxidant (2,2-diphenyl-1-picrylhydrazyl (DPPH) and 2,2´-azinobis (3-ethylbenzothiazoline-6-sulfonic acid) (ABTS)) activities. Among the synthesized compounds, compound **4k** (IC_{50} = 1.18±0.19 µg/mL) emerged as the promising α-Glucosidase inhibitor, significantly outperforming the reference drug Acarbose (IC_{50} = 7.33±0.13µg/mL). For α-Amylase inhibition, compound **4g** (IC_{50} = 13.61±2.04 µg/mL) demonstrated excellent activity, compared to Acarbose (IC_{50} = 43.15±5.22 µg/mL). In antioxidant assays, compound **4o** (IC_{50} = 15.30±1.70 µg/mL) exhibited the strongest DPPH radical scavenging effect, and compound **4g** (IC_{50} = 6.06±0.15 µg/mL) showed the highest ABTS scavenging activity, surpassing the standard antioxidant Trolox (IC_{50} = 30.20±5.14 & 18.19±2.47 µg/mL, respectively). Remarkably, these derivatives showed greater efficacy compared to standard inhibitors, underscoring their promise as novel candidates for antidiabetic and antioxidant drug development. Molecular docking analysis demonstrated strong binding and critical interactions within the enzyme active sites. MD simulations confirmed the stability of **4k**-α-Glucosidase and **4g**-α-Amylase, with RMSD values below 3.6 Å, low RMSF (<2.8 Å) at the binding site, and sustained key interactions with *Phe 158* and *Tyr 151,* respectively. The network pharmacology further supported the findings of molecular docking and simulation analysis.

Keywords; 6-Hydroxychromone; thiosemicarbazones; antidiabetic; antioxidant; enzyme inhibition; molecular docking

1. Introduction

Diabetes mellitus (DM) is a metabolic disorder characterized by inadequate insulin production or impaired insulin function, which in turn disrupts normal carbohydrate and lipid metabolism [1-4]. The rising prevalence of DM has become a major global health issue, significantly impacting human well-being.[5] Type 2 DM accounts for the vast majority of cases, representing over 90 % of all diagnosed cases [6]. Untreated diabetes can result in serious complications like numbness, coma, unconsciousness, and even fatal ketoacidosis.[7] Effective management of Type 2 DM involves a comprehensive approach that involves inhibiting enzymes as α-Amylase and α-Glucosidase, with particular emphasis on controlling postprandial hyperglycemia as a key therapeutic target.[8-11]

α-Glucosidase, a membrane-bound enzyme in the epithelial lining of the human small intestine, is essential in carbohydrate digestion by hydrolyzing terminal 1,4-linked glycosidic bonds in di and polysaccharides to release absorbable monosaccharides.[12] α-Glucosidase inhibitors, a class of oral anti-diabetic drugs, work by competitively binding to the enzyme's active sites, thereby slowing carbohydrate breakdown and reducing glucose absorption in the intestine.[13, 14] Similarly, α-Amylase, a metalloenzyme dependent on calcium, aids carbohydrate digestion by hydrolyzing α-1,4 glycosidic linkages in starch, glycogen, amylose, and amylopectin, producing maltose, maltotriose, and limited dextrins.[15, 16] The final step occurs in the small intestine, where α-Amylase (also known as maltase) breaks down maltose into glucose.[17, 18]

Oxidative stress, implicated in numerous chronic conditions including T2DM, results from the accumulation of reactive oxygen species (ROS), which contain unpaired electrons.[19] These reactive species are produced continuously within the body; although they exhibit certain physiological roles, they can become harmful when present in excess or when the body's

antioxidant defense mechanisms are compromised. In recent years, scientists have focused on the therapeutic potential of antioxidant agents in the prevention and management of diabetes, because free radicals contribute not only to diabetes pathogenesis but also to other serious diseases like cancer, atherosclerosis, and hepatic cirrhosis.[20] Therefore, the discovery of compounds capable of scavenging surplus free radicals is critical for mitigating these life-threatening diseases.[21, 22] Antioxidants play a vital role in protecting cells from oxidative injury.[23]

Chromone, a structurally diverse class of naturally occurring compounds, has shown great potential as a valuable scaffold for designing new drugs.[24-26] These chromone derivatives demonstrate a wide array of pharmacological properties, as antileishmanial, anti-inflammatory, anti-cancer, anti-diabetic and anti-oxidant effects [27, 28]. An emerging field of research has been the significance of the chromone scaffold in medicinal chemistry. Recent advancements in the development of chromone-based therapeutic candidates have led to an increase in the recognition of publications on chromone-based pharmaceuticals. A vast range of compounds with various pharmacological characteristics can be synthesized using chromones as suitable templates for structural changes [29, 30]. They have a significant significance in medicinal chemistry and can be regarded as a preferred structure for drug development because of their structural variety and synthetic accessibility. Moreover, chromone-based drugs have been extensively investigated for asthma therapy, primarily as bronchodilators. These efforts led to the development of disodium cromoglycate (DSCG) and pranlukast (Figure-1), which are clinically used for the treatment of mild-to-moderate asthma and allergic rhinitis, respectively.

Thiosemicarbazones possess a broad spectrum of pharmacological and biological activities, such as antioxidant, antimicrobial, anti-inflammatory, anti-cancer, anti-Alzheimer, and antidiabetic effects, largely attributed to their distinctive (–NH–C(=S)–NH–N=) pharmacophore [31, 32]. Thiosemicarbazones exhibit remarkable antidiabetic activity, showing strong inhibition against enzymes such as dipeptidyl peptidase-4, aldose

reductase (ALR2), α-Glucosidase, glycogen phosphorylase, and α-Amylase.[33, 34] Studies further reveal that conjugation of thiosemicarbazones with diverse heterocyclic frameworks enhances their antidiabetic properties. Similar compounds with chromone and thiosemicarbazone moieties have previously demonstrated significant antidiabetic and antioxidant potential **(Figure-1).**[35-44]

To develop more effective antidiabetic and antioxidant agents, we aimed to synthesize novel hybrid molecules integrating chromone and thiosemicarbazone pharmacophores within a single molecular framework. Based on the hypothesis that combining these two bioactive moieties could synergistically enhance biological activity, we designed and synthesized a series of 6-hydroxychromone-based thiosemicarbazones. The compounds were evaluated for their antidiabetic potential through in vitro enzyme inhibition assays and for antioxidant activity using standard radical scavenging methods. The results demonstrated that several of the synthesized hybrids exhibited promising dual inhibitory effects, supporting their potential as multifunctional therapeutic candidates for managing diabetes and oxidative stress-related conditions.

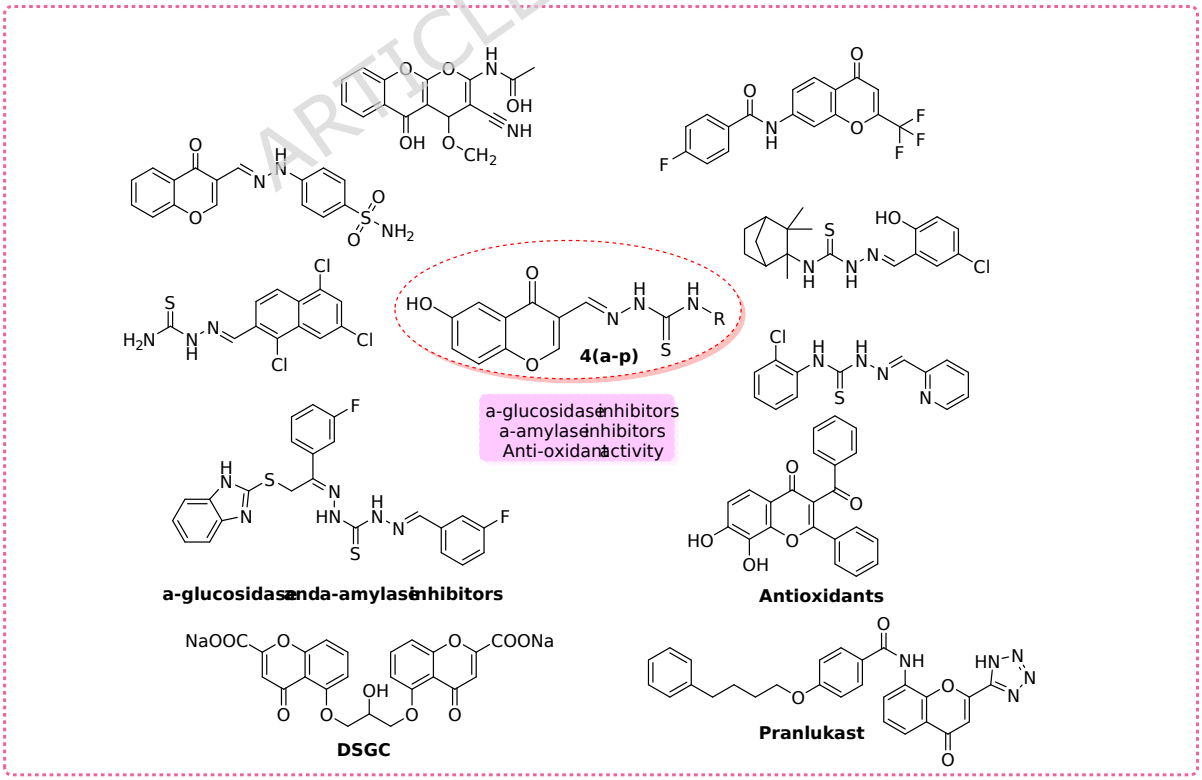

Figure-1: Representative chromone and thiosemicarbazone scaffolds previously reported for enzyme inhibition and antioxidant activity

2. Result and Discussion

2.1. Chemistry

The thiosemicarbazones **4(a-p)** were obtained by reacting 6-hydroxy-4-oxo-4*H*-chromene-3-carbaldehyde **(2)** with a variety of thiosemicarbazides **3(a-p)** in MeOH, and glacial CH_3COOH (2-3 drops) was added to accelerate the reaction. To ensure the reaction completion, TLC was used. The yields of the thiosemicarbazones **4(a-p)** ranged from high to excellent (80–90%). The synthetic route of 6-hydroxychromone-based thiosemicarbazones is demonstrated below (**Scheme-1)**.

Data from ^{1}H NMR and ^{13}C NMR were utilized to determine the structure of the title compounds. The singlet assigned to the NH-N proton at 11 to 12 ppm whereas the NH-CS proton is seen at 10.0 to 10.50 ppm. The hydroxyl peak at 9.0 to 10.0 ppm appeared as a singlet. The methine proton (-CH = N) at 8.0 to 9.0 ppm represents the azomethine group. A singlet at 8.0 to 8.5 ppm represents proton of pyran-4-one ring (-O-CH=). Whereas a doublet at 7.58 and 7.37 ppm and a doublet of doublets at 7.25 ppm represent the chromone ring (compound 4e). A number of peaks in the 7.23–8.28 ppm region is indicative of aromatic protons. The aliphatic protons appear as a singlet, doublet, and triplet at 1 to 4 pm. In the ^{13}C NMR spectrum, the range of 100 –150 ppm corresponds to the aromatic carbons, whereas the C=O carbons are visible at 174 to 177 ppm (chromone) and 177 to 179 ppm (thioamide). The aliphatic carbon appears at 10 to 30 ppm.

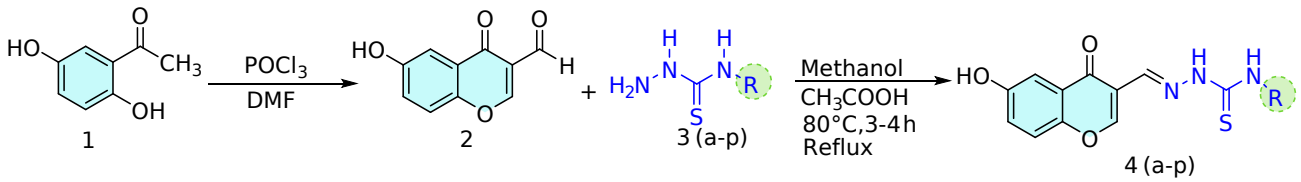

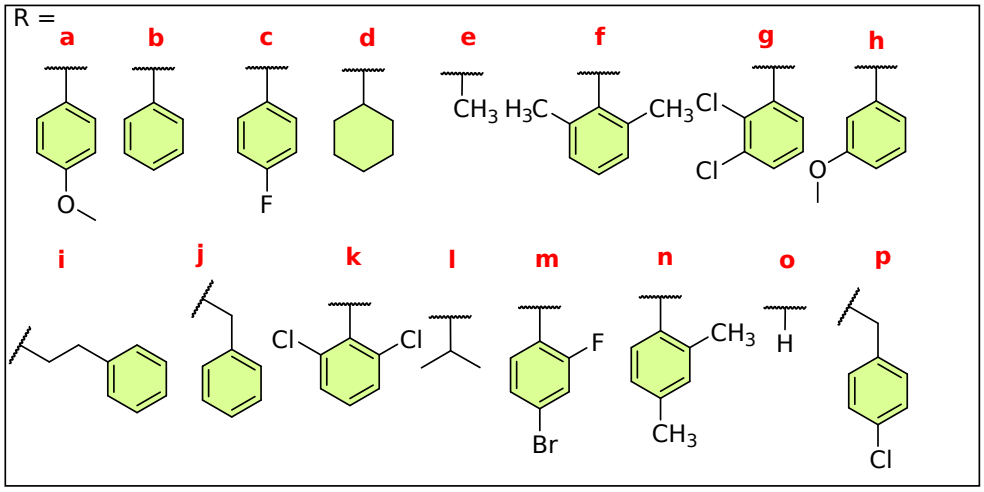

Scheme-1 Synthetic route of Chromone-based thiosemicarbazones **4(a-p)**

2.2. Biological activity

The synthesized compounds exhibited notable α-Glucosidase inhibition (IC_{50} = 1.18±0.19 to 9.30±0.09 µg/mL), where compounds **4c**, **4g**, **4k**, and **4m** outperformed the standard Acarbose (7.33±0.13 µg/mL). For α-Amylase, IC_{50} values ranged from 13.61±2.04 µg/mL to 86.70±2.44 µg/mL, with **4g**, **4k**, and **4p** showing superior activity over Acarbose. In antioxidant assays, DPPH IC_{50} values ranged from 15.30±1.70 µg/mL to 44.36±3.05 µg/mL, and ABTS values ranged from 6.06±0.15 µg/mL to 24.50±3.20 µg/mL, as given in **Table-1**. Compounds **4g**, **4k**, **4o**, and **4p** demonstrated stronger radical scavenging activity compared to Trolox in both assays.

Table-1: The enzymatic and antioxidant activity of compounds **4(a-p)**

Comp.	Enzyme Activity				Antioxidant Activity			
	IC_{50} (µg/mL)							
	α-Glucosidase	**R^2**	**α-Amylase**	**R^2**	**DPPH**	**R^2**	**ABTS**	**R^2**
4a	6.45±0.16	0.938	31.24±1.08	0.930	21.59±0.42	0.908	12.85±1.36	0.935
4b	9.30±0.09	0.927	47.32±5.27	0.939	23.16±1.33	0.962	12.22±0.54	0.966
4c	1.48±0.25	0.983	19.15±2.73	0.927	20.07±1.56	0.901	8.37±2.09	0.908
4d	6.09±0.71	0.931	38.41±1.09	0.931	29.42±3.22	0.942	17.48±1.25	0.925
4e	9.28±0.92	0.928	66.53±7.42	0.984	33.76±1.64	0.938	19.65±2.38	0.906
4f	3.05±0.46	0.927	52.38±4.63	0.951	31.51±2.73	0.957	21.30±2.44	0.915
4g	1.63±0.02	0.964	13.61±2.04	0.967	18.13±1.28	0.916	6.06±0.15	0.974
4h	2.56±0.31	0.954	22.80±3.74	0.974	39.22±3.85	0.929	11.94±2.61	0.965
4i	2.38±0.03	0.971	28.19±1.32	0.951	22.41±2.76	0.933	18.30±3.19	0.907
4j	6.23±0.08	0.981	86.70±2.44	0.907	44.36±3.05	0.902	16.41±2.85	0.912
4k	1.18±0.19	0.960	15.66±4.28	0.930	16.80±0.38	0.994	9.75±1.07	0.920
4l	5.05±0.25	0.917	34.09±2.46	0.967	39.16±1.70	0.957	16.32±4.51	0.938
4m	1.44±0.11	0.962	18.29±3.87	0.935	26.71±3.49	0.948	10.84±1.39	0.906
4n	4.01±0.73	0.965	33.01±5.82	0.934	32.29±6.83	0.973	24.50±3.20	0.965
4o	2.97±0.34	0.939	24.26±4.96	0.987	15.30±1.70	0.927	8.13±0.73	0.991
4p	2.42±0.21	0.971	14.71±2.28	0.986	17.09±2.34	0.936	11.39±1.01	0.909
Acarbose [£]	7.33±0.13	0.938	43.15±5.22	0.947	-	-	-	-
Trolox [¥]	-	-	-	-	30.20±5.14	0.981	18.19±2.47	0.977

2.3. Structure-activity Relationship

2.3.1. Anti-diabetic Activity

2.3.1.1. α-Glucosidase inhibition

The SAR analysis for α-Glucosidase inhibition reveals that the position and nature of substituents on the phenyl ring significantly influence potency. Compounds bearing electron-withdrawing substituents, such as halogens, demonstrate superior potency. For instance, compound **4k** (2,6-dichlorophenyl, IC_{50} = 1.18±0.19 µg/mL), **4c** (4-flourophenyl, IC_{50} = 1.48±0.25 µg/mL), **4g** (2,3-dichlorophenyl, IC_{50} = 1.63±0.02 µg/mL), and **4m** (2-flouro-4-bromophenyl, IC_{50} = 1.44±0.11 µg/mL) exhibit potent α-Glucosidase inhibition. The presence of chlorine and fluorine atoms likely enhances enzyme binding through increased polarity and favourable hydrophobic interactions within the active site. Conversely, compounds with electron-donating groups like **4a** (4-methoxy phenyl, IC_{50} = 6.45±0.16 µg/mL), and **4h** (3-methoxy phenyl, IC_{50} = 2.56±0.31 µg/mL) show moderate activity, suggesting that methoxy substituents contribute to moderate hydrogen bonding but are less effective than halogens. Unsubstituted phenyl **4b** (IC_{50} = 9.30±0.09 µg/mL) and compounds with small alkyl groups like **4e** (methyl, IC_{50} = 9.28±0.92 µg/mL) exhibit weaker inhibitory effects, possibly due to the lack of polar interactions or steric features that optimize enzyme binding. Compounds with non-aromatic substituents such as **4d** (cyclohexyl, IC_{50} = 6.09±0.71µg/mL) and **4l** (isopropyl, IC_{50} = 5.05±0.25 µg/mL) demonstrated moderate inhibition, highlighting the importance of aromaticity for strong enzyme interaction. Compounds with bulky and flexible groups like **4j** (benzyl, IC_{50} = 6.23±0.08 µg/mL) and **4i** (β-phenethyl phenyl, IC_{50} = 2.38±0.03 µg/mL) tend to reduce activity, likely due to the steric hindrance impeding proper fit within the enzyme pocket. Compound **4o** (H, IC_{50} = 2.97±0.34 µg/mL) also shows notable inhibition, indicating the minimal steric bulk can favourably position the core structure for binding. Also, IC_{50} graphs for the best inhibitors in this study are given below **(Figure-2A).**

2.3.1.2. α-Amylase inhibition

Similar trends are observed for α-Amylase inhibition, although some distinctions arise. Compounds with halogen substitutions at 2 and 4 positions, such as **4g** (2,3-dichlorophenyl, IC_{50} = 13.61±2.04 µg/mL), **4k** (2,6-dichlorophenyl, IC_{50} = 15.66±4.28 µg/mL), **4p** (4-chlorophenyl, IC_{50} = 14.71±2.28 µg/mL), showed remarkable potency against α-Amylase. The electron-withdrawing effect of halogens likely enhances interaction with the enzyme active site via hydrophobic and polar contacts. Compound **4c** (4-fluorophenyl, IC_{50} = 19.15±2.73 µg/mL) also displays strong inhibitory activity, supporting the role of electronegativity in enzyme affinity. By contrast, compounds with electron-donating groups, **4f** (2,6-dimethylphenyl, IC_{50} = 52.38±4.63 µg/mL) and 4e (4-methyl, IC_{50} = 66.53±7.42 µg/mL), show weaker inhibition due to the steric hindrance and reduced polarity. Compounds **4h** (3-methoxy phenyl, IC_{50} = 22.80±3.74 µg/mL) showed more potency than compound **4a** (4-methoxy phenyl, IC_{50} = 31.24±1.08 µg/mL) because meta substitution is more effective than para, consistent with electronic effect on enzyme binding. Compound **4d** (cyclohexyl, IC_{50} = 38.41±1.09 µg/mL) and **4l** (isopropyl, IC_{50} = 34.09±2.46 µg/mL) demonstrated moderate activity, suggesting that aromaticity and electronic properties are effective for stronger inhibition. Notably, compound **4o** (H, IC_{50} = 14.71±2.28 µg/mL) also showed relatively strong inhibition, underscoring the benefit of minimal steric hindrance for optimal enzyme interaction. Additionally, **Figure-2B** shows the IC_{50} graphs for the top inhibitors in our investigation.

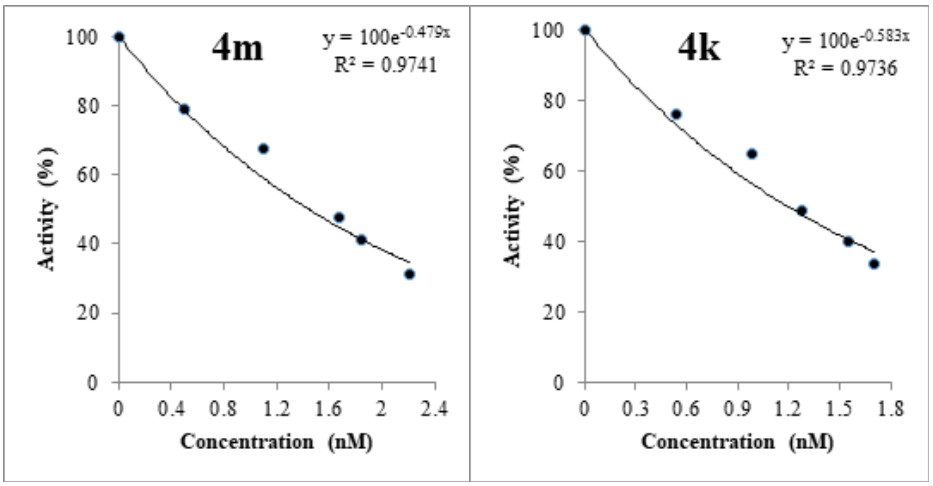

A

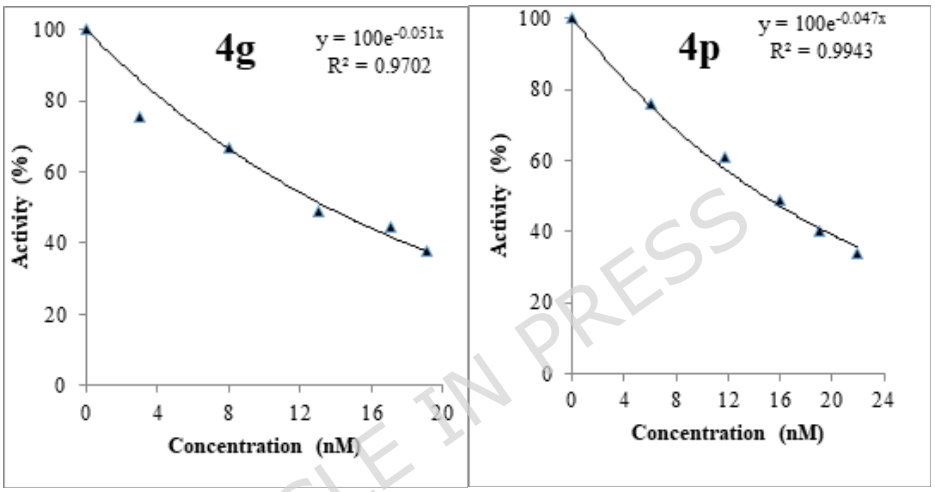

B

Figure-2. (A) IC_{50} graphs of the best inhibitors for α-Glucosidase **(B)** IC_{50} graphs of the best inhibitors for α-Amylase.

2.3.2. Antioxidant Activity

2.3.2.1. DPPH Assay

The DPPH assay shows that compounds bearing halogen substituents, especially chlorine and fluorine, such as **4g** (2,3-dichlorophenyl, IC_{50} = 18.13±1.28 µg/mL), and **4m** (2-fluoro-4-bromophenyl, IC_{50} = 26.71±3.49 µg/mL), demonstrate the strongest antioxidant potential with the lowest IC_{50} values, indicating strong radical scavenging ability. Similarly, **4c** (4-fluorophenyl, IC_{50} = 20.07±1.56 µg/mL) and **4p** (4-chlorophenyl, IC_{50} = 17.09±2.34 µg/mL) also exhibit potent antioxidant effects. Compound **4h (**IC_{50} = 39.22±3.85 µg/mL) with 3-methoxy substitution demonstrated more potency than compound **4a (**IC_{50} = 21.59±0.42 µg/mL) with 4-

methoxy group, suggesting that the methoxy group position influences effectiveness **(Figure-3).** In contrast, alkyl-substituted compounds like **4e** (methyl, IC_{50} = 33.76±1.64 µg/mL), **4f** (2,6-dimethylphenyl, IC_{50} = 31.51±2.73 µg/mL), and **4l** (isopropyl, IC_{50} = 39.16±1.70 µg/mL) show comparatively lower antioxidant activity, likely because electron-donating alkyl groups reduce the ability to stabilize radicals. Compound **4o** (H, IC_{50} = 15.30±1.70 µg/mL) showed moderate activity, indicating the scaffold's intrinsic radical scavenging potential. Overall, the DPPH assay indicates that electron-withdrawing halogen groups enhance antioxidant activity, while electron-donating groups decrease it.

Although α-Glucosidase and α-Amylase catalyze similar glycosidic bond hydrolysis reactions, yet there are noticeable differences between the two. The α-Amylase initiates starch breakdown in the mouth/pancreas and the α-Glucosidase completes the breakdown into monosaccharides in the small intestine. α-Amylase hydrolyzes alpha-1,4-glycosidic bonds in long-chain polysaccharides (starch, glycogen) to produce shorter oligosaccharides and α-Glucosidase breaks down the remaining disaccharides and oligosaccharides into glucose. Even the anti-diabetes drugs such as acarbose and voglibose have different target affinities towards these two enzymes. α-Glucosidase possesses a relatively narrow and well-defined active site that favors stable binding of small-molecule inhibitors. In contrast, α-Amylase contains a broader and more solvent-exposed catalytic groove optimized for polymeric substrates, resulting in weaker and more transient ligand interactions. Similarly, there were also differences in the inhibitory activity observed for these two enzymes in this study, and can be attributed to inherent structural and dynamic differences between the two enzymes. Molecular docking and MD simulation results further support this distinction, as the inhibitors showed more stable binding conformations and lower structural fluctuations within the α-Glucosidase active site compared to α-Amylase. These findings are consistent with previous reports and explain the differential inhibitory activities despite the mechanistic similarity of the two enzymes.

2.3.2.2. ABTS Assay

The ABTS assay confirms similar trends, with halogenated compounds such as **4g** (2,3-dichlorophenyl, IC_{50} = 6.06±0.15 µg/mL, showed the strongest antioxidant activity outperforming the standard Trolox (IC_{50} = 18.19±2.47 µg/mL). Compound **4c** (4-fluorophenyl, IC_{50} = 8.37±2.09 µg/mL) performed better in scavenging ABTS radicals than compound **4p** (4-chlorophenyl, IC_{50} = 11.39±1.01 µg/mL) because of the more electronegative effect of the fluorine group **(Figure-4).** Compound **4a** (4-methoxy, IC_{50} = 12.85±1.36 µg/mL) and **4h** (3-methoxy**,** IC_{50} = 11.94±2.61 µg/mL) show moderate activity, while the meta position showed slightly higher inhibition than 4-mthoxy. Compounds with alkyl substitutions **4e** (methyl, IC_{50} = 19.65±2.38 µg/mL), **4f** (2,6-dimethylphenyl, IC_{50} = 21.30±2.44 µg/mL), and **4l** (isopropyl, IC_{50} = 16.32±4.5 µg/mL) demonstrated weaker antioxidant activity in this assay. Notably, the compound **4o** (H, IC_{50} = 8.13±0.73 µg/mL) showed remarkable potency, reinforcing the intrinsic antioxidant capability of the parent scaffold. The SAR of newly synthesized compounds is depicted in **Figure-4.** The compounds showed a better antioxidant property as compared to previous work Table-2.

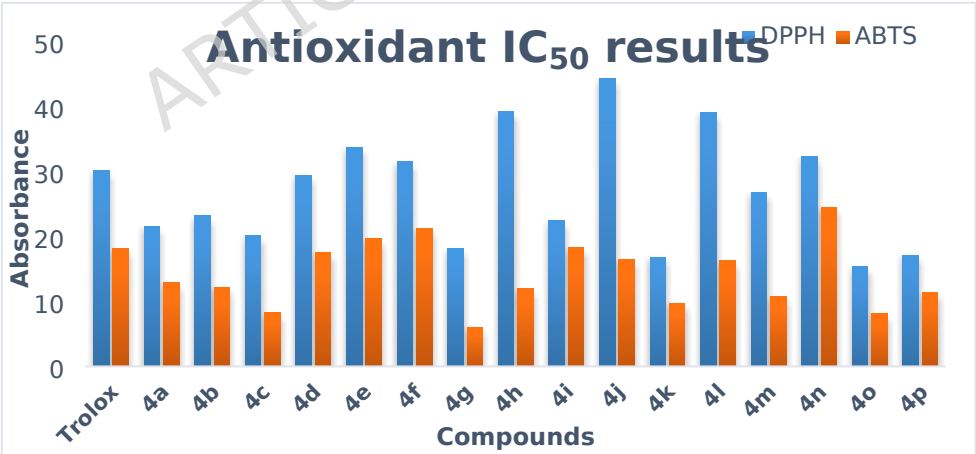

Figure-3. IC_{50} results of the antioxidant for two assays (ABTS and DPPH)

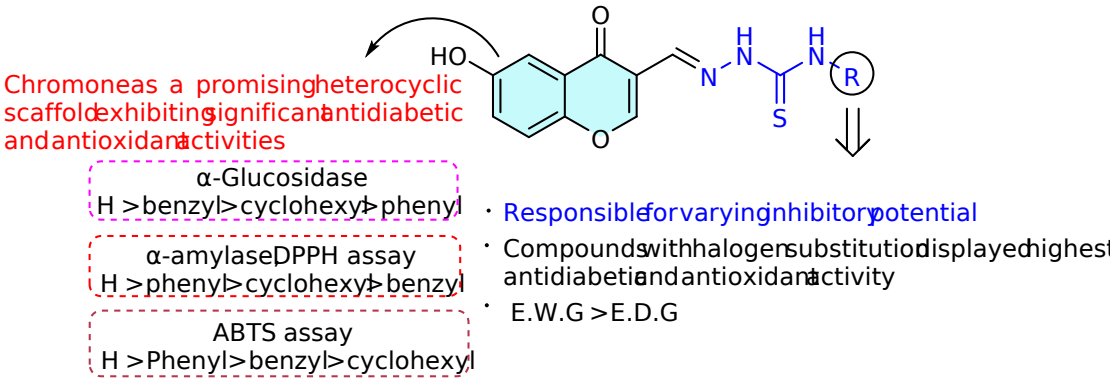

Figure-4. Pictorial representation of **SAR**

Table-2 comparison of antioxidant activity of synthesized compound with other reported work.

Sr. No.	Structure	Antioxidant Activity (IC_{50})	References
1	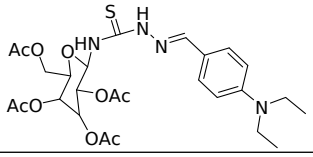	56	[45]
2	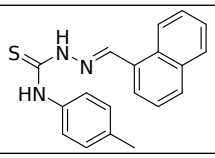	8.631	[46]
3	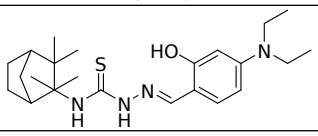	16.78	[47]
4	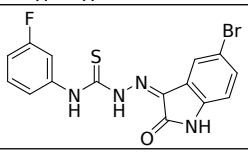	16.42	[48]
5	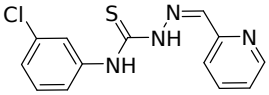	25	[49]
This work	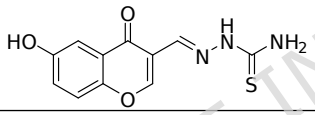	15.30	

2.4. Molecular Docking Studies

The crystal structure of Saccharomyces cerevisiae α-Glucosidase is currently unavailable in the Protein Data Bank; therefore, homology modelling was required. As we previously reported, the homology model was constructed and validated.[50, 51] The oligo-1,6-Glucosidase from *S. cerevisiae,* having PDB ID 3A4A, was found to be a suitable match, which served as a template for the homology modeling. The catalytic triad is formed by amino acids Asp214, Glu276, and Asp349; hence, interaction with these amino acids is critical for substrate binding as well as for enzyme inhibition. Amino acids near the active site (Arg312, His239, His279, Phe231, Asn241, and Glu304) are crucial for binding.

All compounds **4(a-p)** were docked in the enzyme active site; for reference, the standard inhibitor Acarbose was also docked in the same binding site.

The Docking Scores obtained for inhibitors of α-Glucosidase and α-Amylase are given in **Table-S1**.

All the compounds were observed to be oriented in a similar region of the active site, like the standard Acarbose. Overlapping of all compounds with Acarbose is shown in **Figure-5A**.

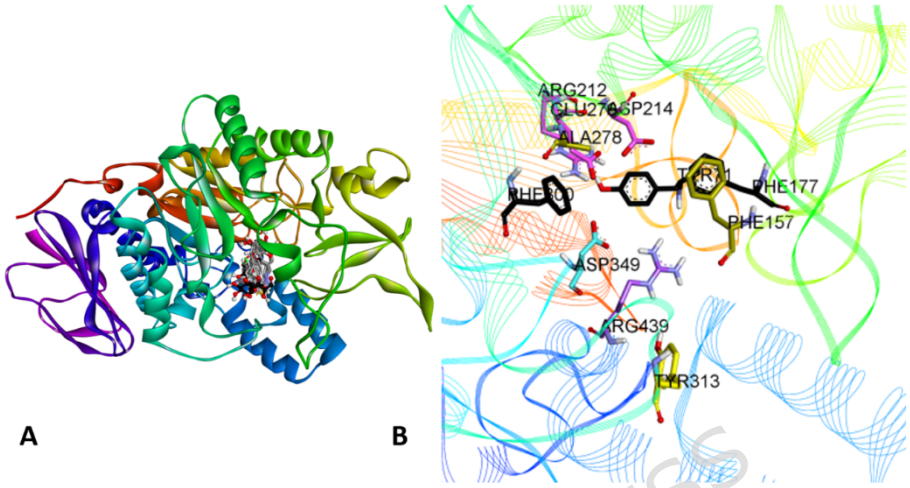

Figure-5. (A) Docked conformations of compounds **4(a-p)** aligned in the α-Glucosidase binding site. The docked conformation of Acarbose is demonstrated in black. **(B)** Common amino acids in the active site interact with the inhibitors.

A detailed analysis of binding modes of all the inhibitors identified important amino acids that frequently interacted with the inhibitors **(Figure-5B).** The amino acids Arg212, Asp214, Glu276, and Phe157 (pink) were frequently engaged in hydrogen bonding contacts with the ligands. Similarly, amino acid Arg439 (purple) was involved in π-cation links with the ligands in a number of compounds. Amino acids Asp349 and Asp214 (cyan) frequently participated in π-anion interactions. Similarly, Phe177, Tyr71, and Phe300 (black) were involved in π-π stacking or T-shaped interactions with the ligands. Ala278 and Phe157 (brown) were involved in alkyl or π-alkyl interactions, indicating their role in stabilizing hydrophobic regions of the binding site. Ligands containing sulfur (S) atoms frequently interact with Tyr313 or Phe177 (yellow) via π-sulfur interactions.

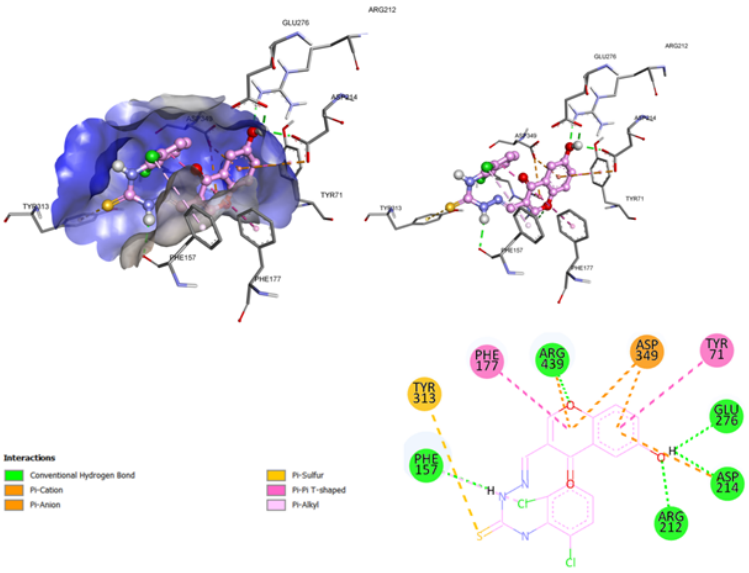

Figure-6. A view of binding site contacts of **4k** in the active site of α-Glucosidase.

Compounds **4k (Figure-6)** and **4c** (**Figure-7)**, being the most active inhibitors, were selected for detailed analysis of binding site interactions. For both compounds **4k** and **4c**, hydrogen-bonded interactions were seen between one of the NH groups and Phe157 **(Table-5**). The OH group linked to the chromone ring also established hydrogen bonds (H-bonds) with Glu276 and Asp214. For compound **4k**, the S-atom of the C=S group was forming a π-sulfur bond with Tyr313, whereas in compound **4c** it was forming an H-bond with Arg312. One of the chloro groups on the Ph- ring was forming a π-alkyl interaction with Phe157; the same Ph- ring was forming an intramolecular π-π T-shaped interaction with the chromone ring. The chromone ring in both compounds was forming π-anion bonds with Asp214 and Asp349, and a π-cation contact with Arg439; for the same ring π-π T-shaped contact with Tyr71 was observed; for compound **4c,** additionally, another π-π T-shaped bond was seen with Phe177. For compound **4c,** the Ph- ring was making a π-π stacked interaction with Phe300 and a π-alkyl interaction with Ala278.

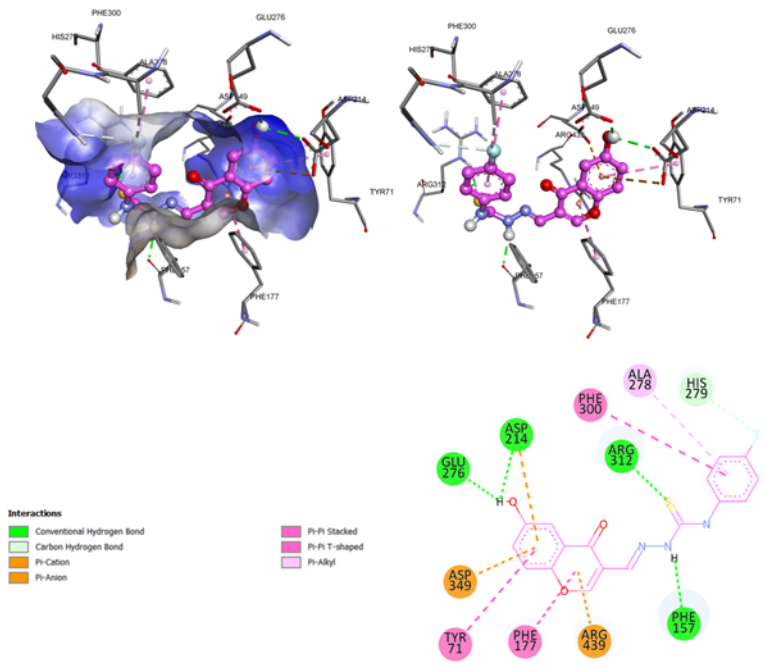

Figure-7. A view of binding site contacts of **4c** (with and without surface representation) in the of α-Glucosidase's active site.

2.5. Molecular Docking Studies of α-Amylase Inhibitors

The crystal structure of human pancreatic α-Amylase in association with inhibitor montbretin A was obtained from the PDB (PDB id: 4w93, 1.35 Å)[52] for docking analysis. The most potent inhibitor, **4g,** was employed for the docking studies. The compound was found to occupy the same binding pocket in the active site as the co-crystallized inhibitor **(Figure-8).**

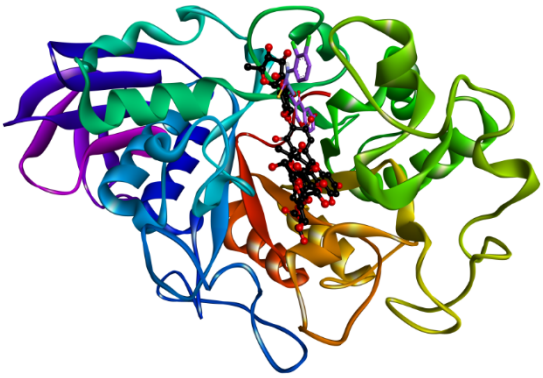

Figure-8. Overlap of docked conformation of α-Amylase inhibitor **4g** with co-crystallized inhibitor (represented in black)

Compound **4g** was the most potent inhibitor of α-Amylase and was therefore chosen for the docking studies **(Figure-9).** The OH group was making an H-bond with lys200. The NH groups were forming H-bonds with Glu240. One of the chloro groups on the Ph- ring was forming a halogen bond with Asn152; this Ph- ring was forming a π-donor interaction with Tyr151. The chromone ring was forming a π-π T-shaped interaction with His201 and a π-π stacked interaction with Tyr151. It also formed a sigma bond with Ile235.

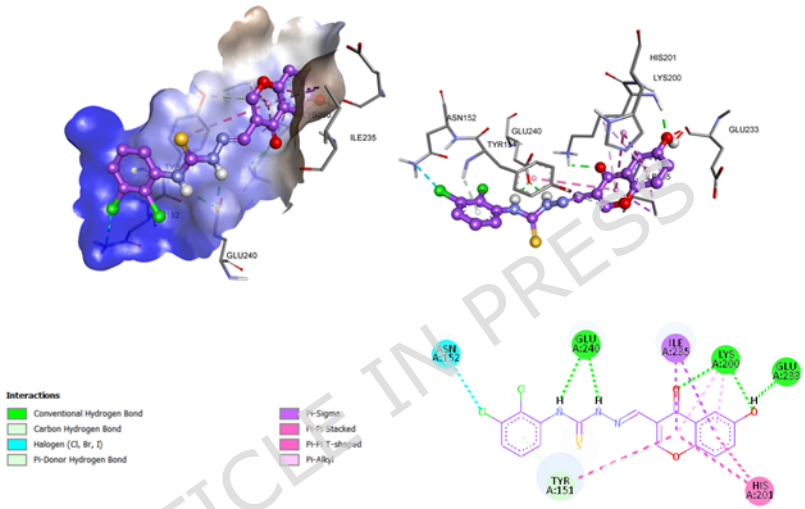

Figure-9. A view of binding site contacts of **4g** (with and without surface representation) in the active site of α-Amylase.

2.6. MD Simulation of α-Glucosidase Inhibitor 4k

The molecular dynamics (MD) analysis of **4k**-α-Glucosidase complex revealed that the RMSD graph of C-α Protein initially rose from 1.3 Å to 3.4 Å within the initial 38 ns, then the value stabilized between 2.8 Å and 3.6 Å and was around 3.2 Å by the completion of the simulation. In the **4k** RMSD graph, the Lig fit on Protein value rose from 2.3 Å to 4.2 Å in the initial 28ns, then the value rose further to 11.6 Å in the next 10ns, then remained between 9 Å to 12.5 Å for the rest of the simulation, and the value stabilized around 11 Å toward the end. The ligand RMSD (Lig fit on Lig) value rose to 2.6 Å during the first 30 ns and remained steady at that value for the duration of the simulation. Protein RMSF analysis revealed

that most residues had fluctuated below 3.0 Å, except *Pro 229* – *Ser 235* with the highest fluctuation by *Lys 233* at 5.17 Å, and *Lys 418* - *Ser 424* with values between 3.2 Å to 3.9 Å. Furthermore, all the residues interacting with the **4k** ligand revealed fluctuations under 2.8 Å. Overall, loop regions of protein structure displayed greater flexibility and dynamic movement. Ligand fit on the Protein RMSF analysis indicated that atoms within **4k** ligand fluctuated between 4 Å to 6.6 Å, with the highest mobility observed for the OH of chromone moiety and Cl atom of chlorobenzene moiety. Protein Secondary Structure analysis indicated % Total SSE = 37.02, where % β-strands = 15.06and % α-helices = 21.96. Protein-Ligand interactions revealed that *Phe 158* demonstrated the highest interaction fraction, exceeding 0.8, primarily through hydrophobic contacts and water bridges.

Ligand-protein contacts reveal that *Phe 158* maintained π-π stacking and hydrophobic interaction with the chromone moiety of **4k** at 19%. *Phe 157* maintained hydrophobic interactions with the thiosemicarbazone moiety at 16%, and *Arg 312* exhibited charged and π-cation interactions with the dichlorobenzene moiety of **4k** at 16%. Ligand **4k**'s torsion profile revealed generally stable torsional behavior across all bonds, with the OH group linked to chromone displayed higher dynamic movement **Figure-10**.

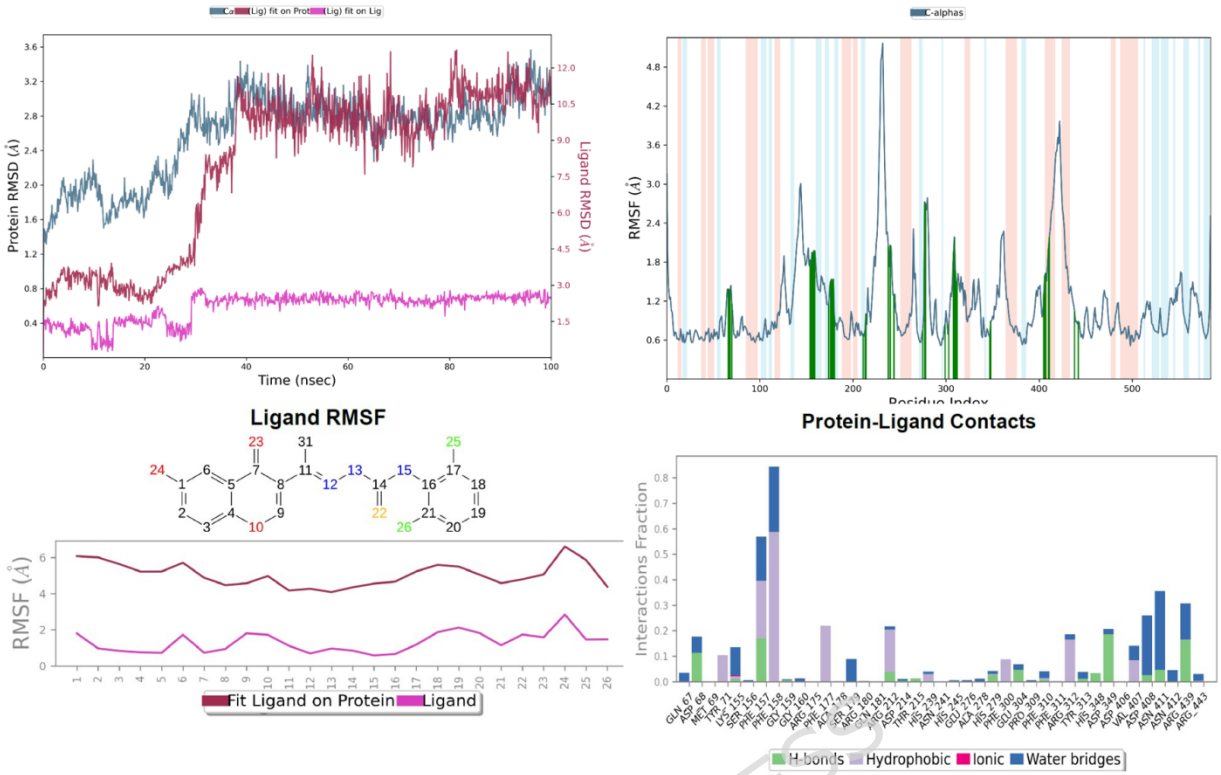

Figure-10. MD simulation studies of **4k**-α-Glucosidase complex for 100ns, RMSD graph, Protein RMSF graph, Ligand RMSF graph, and protein ligand contacts of α-Glucosidase with **4k**.

The MD simulation findings of **4k** with α-Glucosidase indicated that the complex stabilized throughout the whole 100ns simulation time, as the protein RMSD value was observed below 3.6 Å during the whole simulation. However, RMSD values of **4k**, simulation trajectory, Ligand RMSF, as well as torsional profile studies indicated that **4k** displayed dynamic behavior and underwent different conformational, orientational, and positional changes during the simulation. However, lower fluctuation values of residues of α-Glucosidase that made contact with **4k** exhibit that interaction of **4k** with α-Glucosidase contributed to the stabilization of the complex. In general, despite the somewhat dynamic movement of ligand **4k** during the simulation, the complex displayed stable behavior during the simulation **Figure-11**.

Figure 11

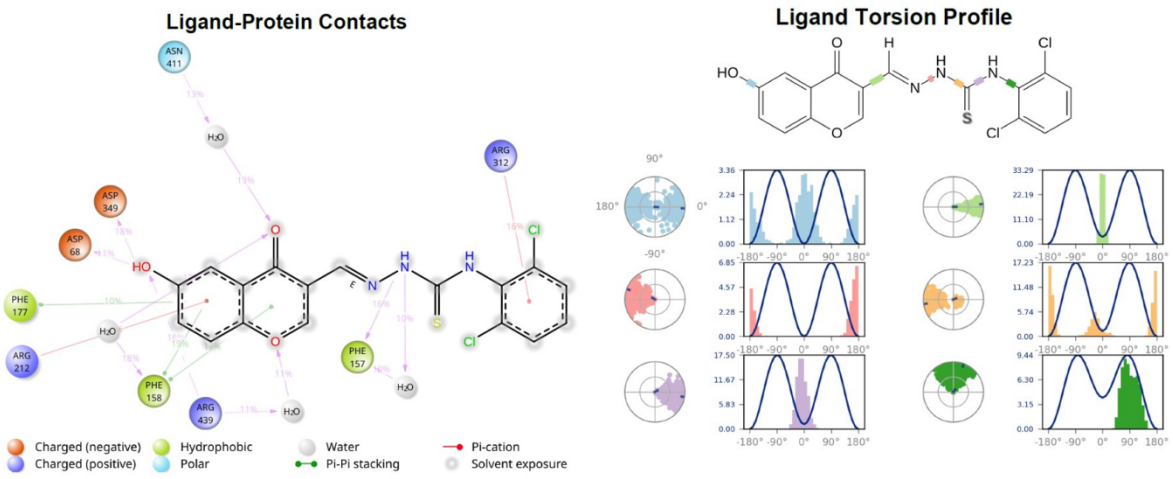

Figure-11. Protein-Ligand Contacts, and Torsional Profile of **4k**-α-Glucosidase complex

2.7. MD Simulation of α-Amylase Inhibitor 4g

The molecular dynamics simulation analysis of **4g**-α-Amylase complex revealed that the C-α Protein RMSD initially rose from 0.8 Å to 2.4 Å within the first 30 ns, after which it stabilized around 2.4 Å for the rest of the simulation. In the RMSD graph of ligand **4g**, the Lig fit on Protein value rose from 2.3 Å to 16.8 Å within the first 28 ns of simulation and then remained fluctuating around 12.0 Å and was observed around 12 Å towards the end of the simulation. **4g**'s Lig fit on lig RMSD value stabilized around 3.2 Å during the simulation duration. Protein RMSF studies revealed that most residues fluctuated below 2.8 Å, except *Ala 307-Gly 309* with values between 4.4 Å – 5.1 Å, *Phe 348-Asn 350* with values between 3.5 Å – 5.9 Å. Furthermore, the α-Amylase residues that directly interact with ligand **4g**, demonstrated values below 2.6 Å. The loop regions of α-Amylase exhibited greater structural flexibility and dynamic fluctuations. Ligand fit on the Protein RMSF graph revealed that atoms of **4g** demonstrated values of fluctuation between 3 Å – 6.1 Å, where atoms of thiosemicarbazone and dichlorobenzene moieties showed relatively lower values around 3 Å, and OH of chromone moiety showed the highest value around 6.1 Å. Protein Secondary Structure elements showed % Total SSE

= 34.60, where % β-strands = 17.76 and % α-helices = 16.84. Among the interacting residues, *Tyr 151* demonstrated the highest interaction frequency (>0.8), characterized mainly by hydrogen bond, hydrophobic, and water bridges interactions. Ligand-protein contacts showed that *Tyr 151* maintained π-π stacking and hydrophobic interactions with chromone moiety around 27% and *His 201* exhibited Polar and π-π stacked contact with dichlorobenzene moiety around 30%. The Ligand torsion profile of **4g** showed that the OH bond of the chromone moiety and the bond between dichlorobenzene and the thiosemicarbazone moiety showed relatively higher dynamic behavior in comparison to the rest of the rotatable bonds in **4g Figure-12**.

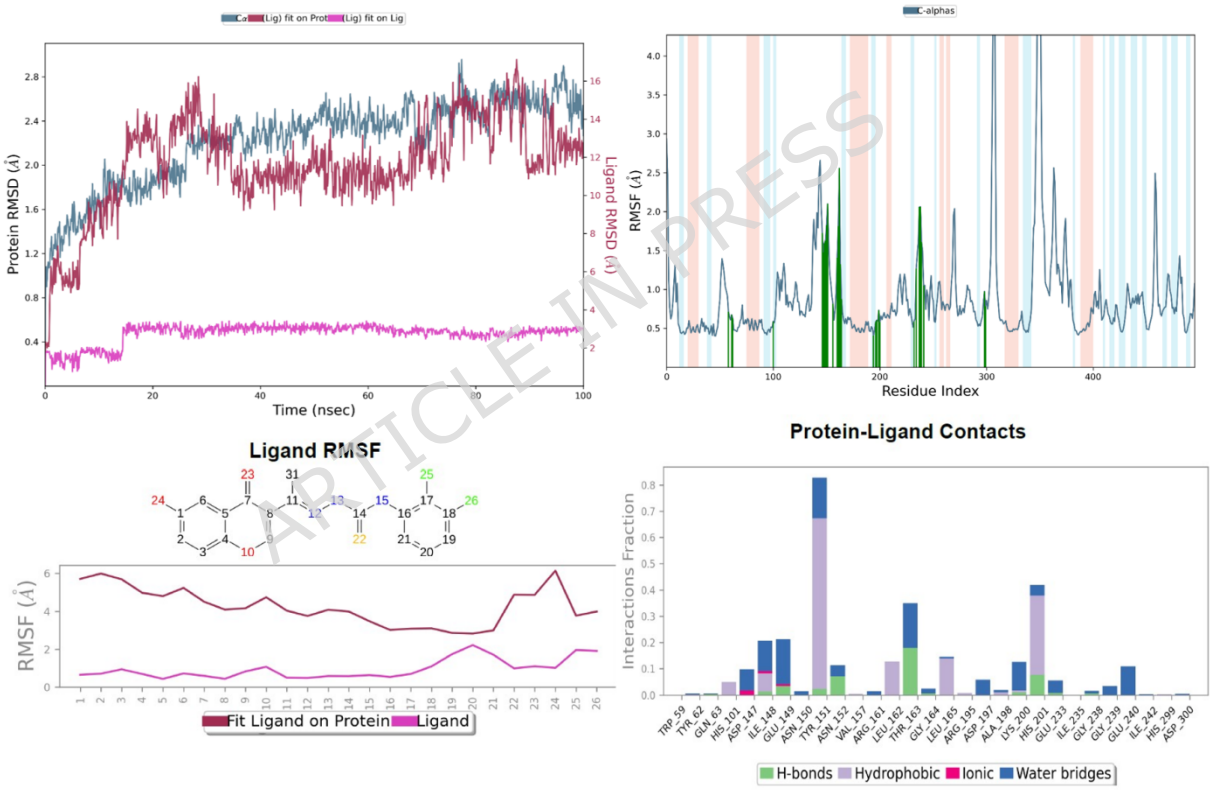

Figure-12. MD simulation analysis of **4g**-α-Amylase complex for 100ns, RMSD plot, Protein RMSF graph, Ligand RMSF graph, and protein ligand **4g**-α-Amylase contacts.

The MD Simulation results of **4g**-α-Amylase revealed that the complex stabilized during the whole 100ns simulation time, as the value of protein RMSD was seen below 3.0 Å throughout the whole simulation. However,

RMSD values of **4g**, the trajectory of simulation, **4g**'s ligand RMSF, as well as torsional profile analysis indicated that **4g** showed different movements during the simulation. The dichlorobenzene moiety of **4g** was observed to orient towards the calcium ion of the α-Amylase as the simulation progressed. Moreover, despite the changes in position, orientation, and conformation of the **4g** during the simulation, the overall complex showed relative stability during the whole simulation. The one common feature observed was the higher RMSF values and torsional behavior of OH groups of both **4k** and **4g** during their respective simulations. The increased RMSF in the loop regions of both α-Amylase and α-Glucosidase may result from the flexible nature of these structural elements **Figure-13**

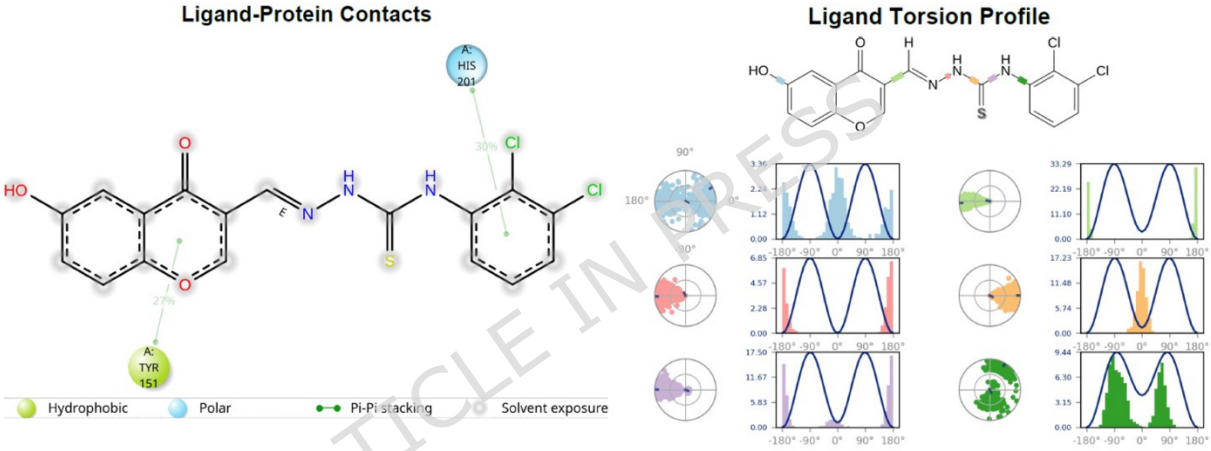

Figure-13. Ligand-Protein Contacts, and Ligand Torsion Profile of **4g**-α-Amylase.

2.8. Post-MD trajectory analysis (PCA, DCCM, and FEL)

The post-MD trajectory analysis tools (Principal Component Analysis PCA, Dynamic Cross-Correlation Matrix DCCM and Free Energy Landscape FEL) were used to understand protein dynamics beyond simple RMSD/RMSF. In PCA graph of protein Cα of 4k α-Glucosidase complex, the first two principal components account for 54.14% of the motion of the protein during the 100ns simulation. PC1 and PC2 account for 41.56% and 12.58% respectively. While in the PCA graph (**Figure S-1 and S-2**) of protein Cα of 4g α-Amylase complex, the initial two principal components express for 43.16% of the movement of protein during the simulation period. Where PC1 and PC2 capturing 34.17% and 8.99% of motion respectively. In the

scatter plots, clusters of frames with clear color transition show both proteins undergone substantive collective motion during their respective simulations, suggesting that both proteins explored different intermediate conformational states during their respective simulations. In eigenvalue graphs of both PCAs, a rapid decrease is observed after the initial principal components in both analyses, indicative of capturing of most part of variance in the limited number of initial dominant components.

DCCM (Dynamic Cross-Correlation Matrix) analysis shows correlation and anti-correlational motion of the residues of the respective proteins. In DCCM graphs of both proteins Cα, for 4k α-Glucosidase complex, the analysis shows widespread portions for the both positive and negative correlations of residues of α-Glucosidase during the simulation period. The specific block-type patterns of correlational and anti-correlational movements could be observed between the residues of the protein. However, in 4g α-Amylase complex, the DCCM graph shows comparatively weak and diffused correlational patterns in residues. In 4g α-Amylase complex, the positive and negative correlational patterns are localized and present in fragments as compared to the block-type regional wide spread patterns of the 4k α-Glucosidase [**Figure S-3 and S-4**].

FEL (Free Energy Landscape) analysis based on RG-RMSD method showed that, in 4k α-Glucosidase complex, a dominant deep low-energy basin can be observed located between 2.50-2.54nm radius of gyration and 0.23-0.27nm of RMSD. In 4g α-Amylase complex, the system exhibits a dominant deep low-energy basin between 2.36-2.39nm of radius of gyration and 0.20-0.25nm of RMSD [Figure S-5 and S-6].

Overall, the complex of 4k α-Glucosidase complex showed more stronger and extensive correlation and anti-correlation movements of the residues as compared to the 4g α-Amylase complex. This suggest that the former complex showing more coordinated global protein residue motions, as compared to the later complex. The PCA analysis indicate that 4k α-Glucosidase displayed more distinct clustering and broader collective movements, while 4g α-Amylase complex showed continuous and restricted distributions. FEL analysis also showed that both complexes and

systems converged to a defined low-energy basins, indicating that both of these reached the stable conformational state during the respective simulation periods.

2.9. *In-silico* ADME Analysis

To evaluate the drug likeness of compounds, *in silico* ADME properties were assessed utilizing SwissADME (**Table-3**). The number of rotatable bonds in a molecule serves as a measure of flexibility in a molecule. According to Veber's rule, which outlines criteria for oral bioavailability, the number of rotatable bonds should not exceed 10; this criterion was observed by all compounds described herein **4(a-p).** Compound **4o** had the least number of rotatable bonds (3), compound **4e** had 4 rotatable bonds, and compound **4i** had 7 rotatable bonds. Compounds **4a**, **4h**, **4j,** and **4l** had 6 rotatable bonds, while the remaining compounds (**4b**-**4d**, **4f**, **4g**, **4k**, **4m,** and **4p**) had 5 rotatable bonds. The ideal value of topological polar surface area (TPSA) should not be more than 140; all compounds had favorable TPSA values of 118-132. Consequently, all compounds were predicted to have high gastrointestinal absorption and were not BBB permeant. The number of H-bond donors (3) and acceptors (4-5) was also within the allowed range. Compounds **4e** and **4o** were the only compounds that were predicted to be water soluble, while most other compounds are expected to be moderately to poorly soluble.

Table-3. *In silico* ADME properties of compounds, No. Of rotatable bonds (RtB), number of H-bond acceptors and donors (H-BA and #H-BD), **4(a-p).**

Code	#RtB	#H-BA	#H-BD	TPSA	Log P	Solubility	GI	BBB
4a	6	5	3	128.18	2.49	Moderately soluble	High	No
4b	5	4	3	118.95	2.5	Moderately soluble	High	No
4c	5	5	3	118.95	2.81	Poorly soluble	High	No
4d	5	4	3	118.95	2.62	Moderately soluble	High	No
4e	4	4	3	118.95	1.23	Soluble	High	No
4f	5	4	3	118.95	3.12	Poorly soluble	High	No
4g	5	4	3	118.95	3.56	Poorly soluble	High	No
4h	6	5	3	128.18	2.49	Moderately soluble	High	No
4i	7	4	3	118.95	2.79	Poorly soluble	High	No
4j	6	4	3	118.95	2.56	Poorly soluble	High	No
4k	5	4	3	118.95	3.54	Poorly soluble	High	No
4l	6	4	3	118.95	2.19	Moderately soluble	High	No
4m	5	5	3	118.95	3.45	Poorly soluble	High	No
4n	5	4	3	118.95	3.15	Poorly soluble	High	No
4o	3	4	3	132.94	0.89	Soluble	High	No
4p	5	4	3	118.95	3.04	Poorly soluble	High	No

None of the compounds were predicted to be substrates for P-glycoprotein **(Table-4),** indicating they will not be affected by Pgp efflux transport and will not be easily effluxed out of the cells, which is a desirable trait for drug-like molecules. Cytochrome P450 (CYP) enzymes are involved in the drug detoxification mechanism; most of the known drugs are acted upon by these enzymes to convert them into water-soluble compounds so they can be excreted out of the body. Compound **4o** was the only compound that was predicted not to inhibit CYP1A2, while all other compounds are predicted to inhibit this detoxification enzyme, hinting at possible drug-drug interactions. Only compounds **4d**, **4i,** and **4j** were predicted to inhibit CYP2C19, while the rest of the compounds are predicted not to interfere with its function. Most of the compounds were predicted to inhibit CYT2C9 and CYT3A4, indicating increased drug toxicity, which can be countered by appropriate drug dosage. None of the compounds was predicted to inhibit CYT2D6.

Table-4. Predicted pharmacokinetic properties of compounds **4(a-p).**

Code	Pgp substrate	CYP1A2 inhibitor	CYP2C19 inhibitor	CYP2C9 inhibitor	CYP2D6 inhibitor	CYP3A4 inhibitor
4a	No	Yes	No	Yes	No	Yes

4b	No	Yes	No	Yes	No	Yes
4c	No	Yes	No	Yes	No	Yes
4d	No	Yes	Yes	Yes	No	Yes
4e	No	Yes	No	No	No	No
4f	No	Yes	No	Yes	No	Yes
4g	No	Yes	No	Yes	No	Yes
4h	No	Yes	No	Yes	No	Yes
4i	No	Yes	Yes	Yes	No	Yes
4j	No	Yes	Yes	Yes	No	Yes
4k	No	Yes	No	Yes	No	Yes
4l	No	Yes	No	Yes	No	No
4m	No	Yes	No	Yes	No	Yes
4n	No	Yes	No	Yes	No	Yes
4o	No	No	No	No	No	No
4p	No	Yes	No	Yes	No	Yes

2.10. Network Pharmacology Analysis

The Venn diagram analysis (**Figure 14**) illustrated the comparison between compound-predicted and disease-associated genes, where panel A represents 65 predicted genes from DIGEP-Pred ($p > 0.5$) and panel B depicts 181 targets retrieved from GeneCards (GIFt score > 65). The intersection of both datasets identified 11 common genes, signifying strong molecular relevance to both antioxidant and antidiabetic mechanisms. These 11 overlapping genes, such as TP53, KRAS, CFTR, RAF1, IGF1R, PDGFRB, CREBBP, TGFBR1, FGFR2, CHEK1, and CDK5, were found to be interconnected in regulating both diabetic and antioxidant responses, as supported by their annotation in GeneCards, where each was listed under both antioxidant proteins and diabetes-related gene categories [53, 54].

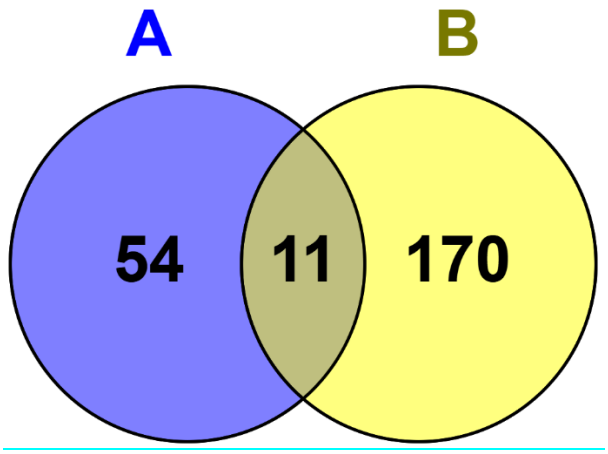

Figure 14: The Venn analysis: Panel **A** represents 65 predicted genes from DIGEP-Pred ($p > 0.5$), and Panel **B** depicts 181 targets retrieved from GeneCards (GIFt score > 65).

KEGG pathway enrichment demonstrated that these targets are primarily involved in key metabolic and signaling networks regulating insulin response and oxidative stress balance. A systematic framework of network pharmacology was presented in **Figure 15** to elucidate how bioactive compounds exert therapeutic effects through multi-target interactions rather than single-receptor mechanisms. This approach is particularly valuable in understanding complex diseases like diabetes, where metabolic dysregulation and oxidative stress are closely interlinked. Mapping these interconnected networks highlights how perturbations at one molecular node can propagate through the system, ultimately restoring or disrupting metabolic balance.

Several molecular signaling routes simultaneously contribute to the development of diabetes and the regulation of oxidative balance, providing a mechanistic link between metabolic stress and cellular defense. Among these, the PI3K-Akt and AMPK pathways (hsa04151 and hsa04152) play central roles in maintaining glucose homeostasis and energy balance while modulating redox-sensitive transcription factors such as FoxO and Nrf2. The activation of AMPK under conditions of nutrient deprivation enhances antioxidant capacity through the upregulation of superoxide dismutase and catalase, while PI3K-Akt signaling influences insulin sensitivity and inhibits excessive ROS accumulation. Components such as IGF1R, CDK5,

and CREBBP integrate into these cascades, affecting insulin signaling, cell survival, and mitochondrial function, which are often compromised during the progression of type 2 diabetes. The MAPK (hsa04010) and p53 (hsa04115) signaling pathways also intersect with diabetic and oxidative stress responses. MAPK signaling, regulated by upstream mediators like KRAS and RAF1, responds to hyperglycemic conditions by controlling cell proliferation and inflammatory signaling, but it also activates stress-related kinases that promote the expression of antioxidant genes through Nrf2 and AP-1. Similarly, p53 functions as a redox-sensitive transcription factor that can either induce antioxidant enzymes such as GPX and SOD under mild stress or promote apoptosis in the presence of severe oxidative imbalance. The tumor suppressor TP53 and the checkpoint kinase CHEK1 together maintain DNA stability under oxidative and metabolic stress, mechanisms that are disrupted in diabetic complications. Transforming growth factor β and fibroblast growth factor cascades (hsa04350, hsa04066) further contribute to redox and metabolic control through TGFBR1 and FGFR2[55, 56]. Compounds **4g**, **4o**, and **4k**, which engage multiple targets within these networks, highlight this interplay between metabolism and oxidative regulation. Compound 4g primarily acts on PDGFRB, linking vascular remodeling and oxidative signaling seen in the AGE-RAGE pathway (hsa04933). Compound **4k** targets PDGFRB and CDK5, aligning with the PI3K-Akt (hsa04151) and AMPK (hsa04152) pathways that modulate insulin release and antioxidant capacity. The most versatile, compound **4o**, interacts with TP53, KRAS, CFTR, RAF1, IGF1R, PDGFRB, CREBBP, TGFBR1, FGFR2, CHEK1, and CDK5, connecting to the MAPK (hsa04010), FoxO (hsa04068), p53 (hsa04115), and TGF-beta (hsa04350) pathways. Through these interactions, **4o** may influence insulin sensitivity, ROS detoxification, and cellular resilience, illustrating how multitarget engagement within a network pharmacology framework can yield synergistic therapeutic effects against diabetes-associated oxidative stress.

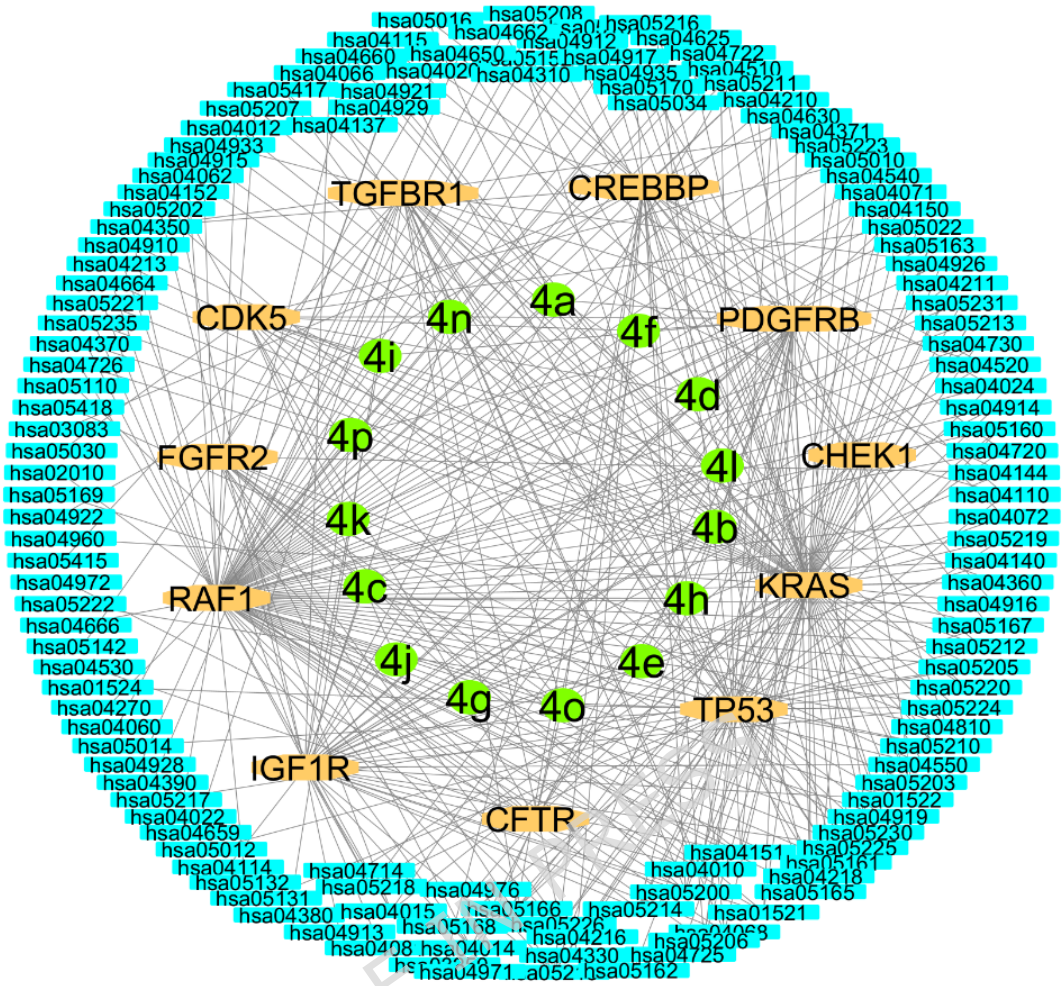

Figure 15: A schematic representation of Network pharmacology highlighting Compound-Target (C-T) and Target-Pathway (T-P) interactions. Compounds, Targets, and Pathway Ids are colored as green, brown, and cyan, respectively.

The **Gene Ontology (GO) enrichment analysis** illustrated in **Figure 16** highlights the major biological processes (A), cellular components (B), and molecular functions (C) associated with the identified common target genes linked to diabetes and antioxidant properties. Panel A demonstrated that the enriched biological processes predominantly involve the cellular response to transforming growth factor beta (TGF-β) stimulus with a fold enrichment of around 35 and a -log10(FDR) value close to 8. In addition to this, peptidyl-amino acid modification shows a fold enrichment of approximately 25 with a -log10(FDR) near 7, and protein phosphorylation with a fold enrichment of nearly 20 and a -log10(FDR) value around 6. Panel B revealed that the most significantly enriched cellular components

include the protein kinase 5 complex, exhibiting a fold enrichment of 600. Similarly, the transforming growth factor beta ligand-receptor complex, with a fold enrichment around 500 and -log10(FDR) close to 2.0, and the insulin receptor complex, showing a fold enrichment near 450 and -log10(FDR) value of about 1.8, further emphasize the importance of receptor-mediated and kinase-associated pathways that are directly linked to glucose metabolism and oxidative regulation. Panel C highlighted the predominant molecular functions such as growth factor binding, protein kinase activity, and ATP binding with a fold enrichment of about 30-75 and -log10(FDR) of 5.0-7.0. These molecular functions indicate strong kinase-driven signaling and energy-dependent activities crucial for maintaining redox balance and enhancing insulin response. Overall, the GO enrichment data suggest that these shared genes are mainly involved in kinase-mediated signaling, growth factor interactions, and phosphorylation events, all of which are critical in regulating oxidative stress and improving insulin sensitivity in diabetic pathophysiology.

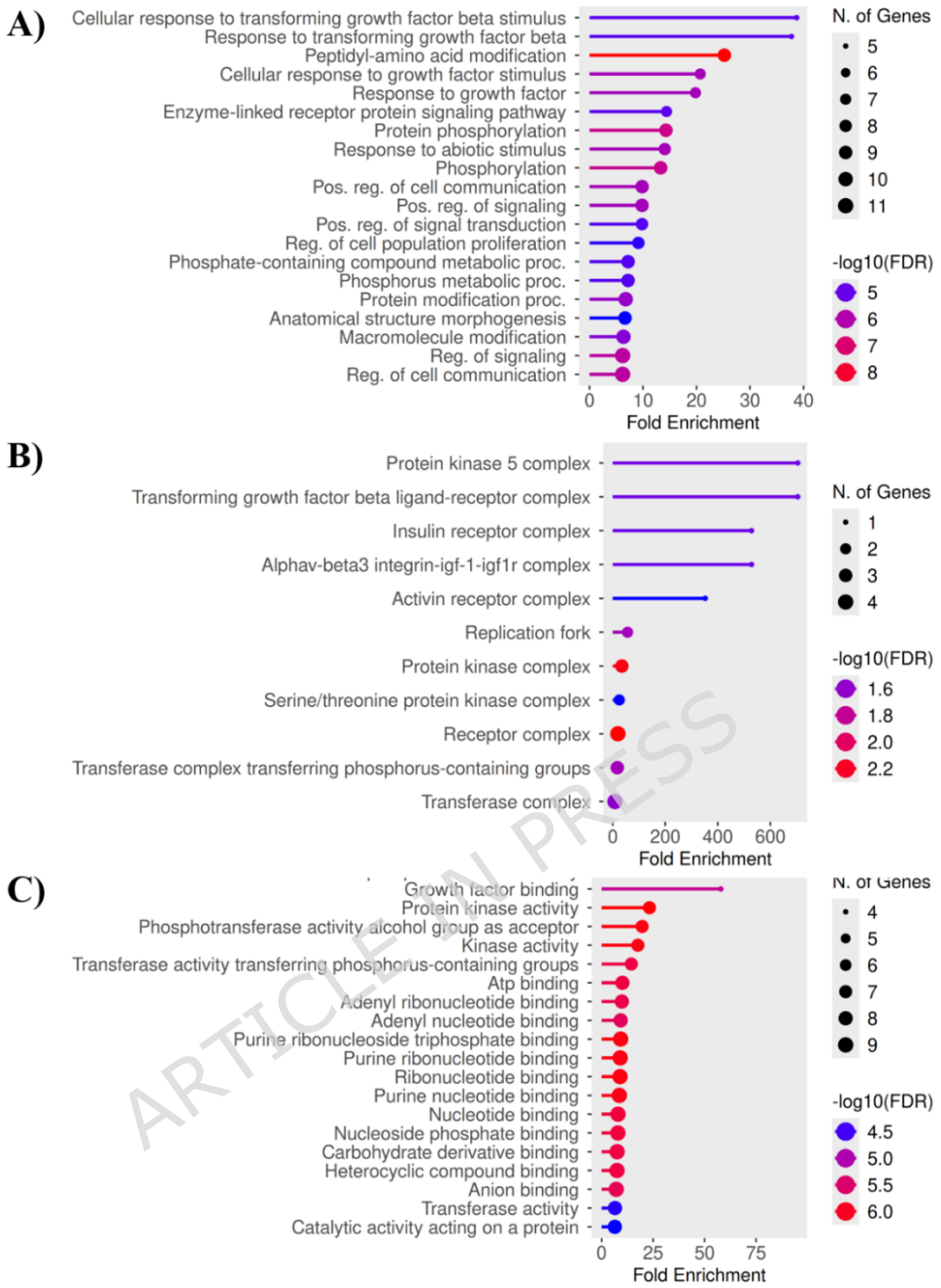

Figure 16: The GO-enrichment analysis: **A)** Biological processes, **B)** Cellular Functions, **C)** Molecular Functions

3. Experimental

3.1. General

The materials used in this research were obtained from commercial suppliers, like Fluka, Oakwood, as well as Sigma Aldrich, and applied directly without further processing. Analytical-grade solvents, such as EtOH, n-hexane, and CH_3COOH, were purchased from Merck and employed directly in the experimental procedures without additional

purification. TLC was employed to monitor the reaction using pre-coated silica gel plates. Petroleum ether and ethyl acetate (3:1) were used as the solvent system, and spots were observed under UV light at 254 nm. TMS is used as the internal standard, and DMSO-d6 is used as the solvent. ^{1}H NMR and ^{13}C NMR spectra using Bruker 400 MHz (Bruker Avance III HD 400MHz) and 101 MHz spectrophotometers, respectively. Coupling constants (J) were given in Hertz (Hz), as well as chemical shifts were described in ppm. High-resolution mass spectrometry (HRMS) spectra were obtained using the electrospray ionization (ESI) technique on a Thermo Fisher Scientific Q Exactive™ Hybrid Quadrupole-Orbitrap™ instrument.

3.2. General procedure for the synthesis of 6-hydroxy-4-oxo-4*H*-chromene-3-carbaldehyde (2)

Chromone carboxaldehyde (2) was synthesized by the Vilsmeier-Haack reaction using 2-hydroxyacetophenone. The formylating agent, also known as the Vilsmeyer-Haack Reagent (chloroiminium), is formed *in situ* from DMF and phosphorus oxychloride. The acetyl group of hydroxyacetophone undergo enolization under acidic conditions, generating a nucleophilic enol/enolate which attacks the electrophilic carbon of the chloroiminium, forming a β-chloroiminium intermediate followed by attack of hydroxyl group at activated carbon resulting in ring clouser. Finally, the hydrolysis of the intermediate resulted in the formation of 6-hydroxy-3-formyl chromone (2).

Typically, $POCl_3$ (4 ml, 42.9 mmol) was added dropwise to DMF (20 ml) [36]. The mixture was stirred at 50 °C for 2 h. After that, a solution of 2,5-dihydroxyacetophenone (10 mmol) in DMF (2 ml) was added to the reaction mixture and was further heated at 50 °C for 2 h. TLC was employed to check the reaction progress. Upon completion, the resulting mixture was poured into iced H_2O while constantly stirring. The resulting precipitates were filtered and washed with cold H_2O to yield 6-hydroxy-4-oxo-4*H*-chromene-3-carbaldehyde as a yellow solid.

3.3. General procedure for synthesis of thiosemicarbazones 4(a-p)

Chromone-based thiosemicarbazones **4(a-p)** were synthesized by reacting 6-hydroxy-4-oxo-4*H*-chromene-3-carbaldehyde **(2)** (1 mmol) with substituted thiosemicarbazides **3(a-p)** (1 mmol) in methanol (10 ml) by adding acetic acid (2-3 drops) for 2-3 h at 80 °C [57]. The reaction's progress was monitored via TLC. The resulting precipitates were filtered, rinsed with methanol, and dried. The targeted thiosemicarbazones **4(a–p)** were obtained in excellent yields (80–90%). Final purification was performed by recrystallization using chloroform, yielding pure compounds **4(a-p).**

(*E*)-2-[(6-Hydroxy-4-oxo-4*H*-chromen-3-yl)methylene]-*N*-(4-methoxyphenyl) hydrazine-1-carbothioamide (4a)

Color: light-yellow; Yield: 87 %, m.p.: 235-237 °C; δ_H ^{1}H NMR (400 MHz, DMSO) δ 11.84 (s, 1H, C=N-NH), 10.12 (s, 1H, S=C-NH), 10.01 (s, 1H, -OH), 9.27 (s, 1H, CH=N), 8.29 (s, 1H, -O-CH=C), 7.59 (d, J = 9.0 Hz, 1H, Ar-H), 7.46 – 7.27 (m, 3H, Ar-H), 7.27 (dd, J = 9.0, 3.0 Hz, 1H, Ar-H), 6.95 (d, J = 8.9 Hz, 2H, Ar-H), 3.78 (s, 3H, OCH_3). ^{13}C NMR (101 MHz, DMSO) δ 176.79, 175.06, 157.50, 155.77, 149.98, 135.31, 132.32, 128.00, 124.79, 123.82, 120.59, 117.57, 113.81, 108.21, 55.73. ESI-HRMS: m/z Formula: $C_{18}H_{15}N_3O_4S$, calculated $[M+H]^+$: 369.07833, found $[M+H]^+$: 370.08548.

(*E*)-2-[(6-Hydroxy-4-oxo-4*H*-chromen-3-yl)methylene]-*N*-phenylhydrazine-1-carbothioamide (4b)

Color: light-yellow; Yield: 80 %, m.p.: 243-245 °C; δ_H (400 MHz, DMSO) 11.92 (s, 1H, C=N-NH), 10.12 (s, 1H, S=C-NH), 9.28 (s, 1H, -OH), 8.32 (s, 1H, CH=N), 7.65 – 7.52 (m, 3H, Ar-H), 7.44 – 7.35 (m, 3H, Ar-H), 7.31 – 7.19 (m, 2H, Ar-H). ^{13}CNMR (101 MHz, DMSO) δ 176.40, 175.06, 155.87, 155.79, 149.99, 139.44, 135.64, 128.58, 126.30, 125.88, 124.79, 123.84, 120.59, 117.51, 108.23. ESI-HRMS: m/z Formula: $C_{17}H_{13}N_3O_3S$, calculated $[M+H]^+$: 339.06776, found $[M+H]^+$: 340.07482.

(*E*)-*N*-(4-Fluorophenyl)-2-[(6-hydroxy-4-oxo-4*H*-chromen-3-yl)methylene]hydrazine-1-carbothioamide (4c)

Color: light-yellow; Yield: 82 %, m.p.: 238-240 °C; δ_H (400 MHz, DMSO) 11.95 (s, 1H, C=N-NH), 10.13 (s, 1H, S=C-NH), 9.26 (s, 1H, -OH), 8.31 (s, 1H, CH=N), 7.63 – 7.51 (m, 3H, Ar-H), 7.40 (d, J = 3.0 Hz, 1H, -O-CH=C),

7.31 – 7.17 (m, 3H, Ar-H). ^{13}C NMR (101 MHz, DMSO) δ 176.76, 175.05, 161.39, 158.98, 155.82, 155.79, 149.98, 135.79, 135.75, 128.58, 128.49, 124.79, 123.84, 120.59, 117.50, 115.37, 115.14, 108.22. ESI-HRMS: m/z Formula: $C_{17}H_{12}FN_3O_3S$, calculated $[M+H]^+$: 357.05834, found $[M+H]^+$: 358.06511.

(*E*)-*N*-Cyclohexyl-2[(6-hydroxy-4-oxo-4*H*-chromen-3-yl)methylene]hydrazine-1-carbothioamide (4d)

Color: white; Yield: 86 %, m.p.: 241-243 °C; δ_H (400 MHz, DMSO) 11.49 (s, 1H, C=N-NH), 10.10 (s, 1H, S=C-NH), 9.13 (s, 1H, -OH), 8.20 (s, 1H, CH=N), 8.04 (d, J = 8.6 Hz, 1H, -O-CH=C), 7.59 (d, J = 9.0 Hz, 1H, Ar-H), 7.38 (d, J = 3.0 Hz, 1H, Ar-H), 7.26 (dd, J = 9.0, 3.0 Hz, 1H, Ar-H), 4.20 (dtd, J = 10.8, 7.3, 4.1 Hz, 1H, Cyclohexyl), 1.89 (dd, J = 12.2, 3.9 Hz, 2H, Cyclohexyl), 1.75 (dt, J = 12.8, 3.3 Hz, 2H, Cyclohexyl), 1.63 (dd, J = 12.6, 4.1 Hz, 1H, Cyclohexyl), 1.48 – 1.21 (m, 4H, Cyclohexyl). ^{13}C NMR (101 MHz, DMSO) δ 176.14, 175.05, 155.74, 155.44, 149.96, 134.94, 124.76, 123.80, 120.54, 117.57, 108.20, 53.13, 32.41, 25.68, 25.44. ESI-HRMS: m/z Formula: $C_{17}H_{19}N_3O_3S$, calculated $[M+H]^+$: 345.11471, found $[M+H]^+$: 346.12177.

(*E*)-2-[(6-Hydroxy-4-oxo-4*H*-chromen-3-yl)methylene]-*N*-methylhydrazine-1-carbothioamide (4e)

Color: light-yellow; Yield: 90 %, m.p.: 249-251 °C; δ_H (400 MHz, DMSO) 11.57 (s, 1H, C=N-NH), 10.10 (s, 1H, S=C-NH), 9.06 (s, 1H, -OH), 8.54 (d, J = 4.7 Hz, 1H, CH=N), 8.19 (s, 1H, -O-CH=C), 7.59 (d, J = 9.1 Hz, 1H, Ar-H), 7.38 (d, J = 3.0 Hz, 1H, Ar-H), 7.26 (dd, J = 9.0, 3.0 Hz, 1H, Ar-H), 3.03 (d, J = 4.5 Hz, 3H, -N-CH_3). ^{13}C NMR (101 MHz, DMSO) δ 178.24, 175.06, 155.73, 155.03, 149.96, 134.37, 124.75, 123.80, 120.55, 117.78, 108.18. ESI-HRMS: m/z Formula: $C_{12}H_{11}N_3O_3S$, calculated $[M+H]^+$: 277.05211, found $[M+H]^+$: 278.05907.

(*E*)-*N*-(2,6-Dimethylphenyl)-2-[(6-hydroxy-4-oxo-4*H*-chromen-3-yl)methylene] hydrazine-1-carbothioamide (4f)

Color: white; Yield: 88 %; m.p.: 237-239 °C, δ_H (400 MHz, DMSO) 11.84 (s, 1H, C=N-NH), 10.13 (d, J = 1.3 Hz, 1H, S=C-NH), 9.87 (s, 1H, -OH), 9.25 (s, 1H, CH=N), 8.30 (s, 1H, -O-CH=C), 7.58 (d, J = 9.0 Hz, 1H, Ar-H), 7.40

(d, J = 3.0 Hz, 1H, Ar-H), 7.26 (dd, J = 9.0, 3.0 Hz, 1H, Ar-H), 7.13 (d, J = 2.1 Hz, 3H, Ar-H), 2.20 (s, 6H, -CH_3). ^{13}C NMR (101 MHz, DMSO) δ 177.25, 175.07, 155.74, 155.64, 150.01, 137.43, 136.93, 134.87, 128.09, 127.45, 124.80, 123.79, 120.58, 117.69, 108.22, 18.51. ESI-HRMS: m/z Formula: $C_{19}H_{17}N_3O_3S$, calculated $[M+H]^+$: 367.09906, found $[M+H]^+$: 368.10600.

(*E*)-*N*-(2,3-Dichlorophenyl)-2-[(6-hydroxy-4-oxo-4*H*-chromen-3-yl)methylene]hydrazine-1-carbothioamide (4g)

Color: white; Yield: 87 %, m.p.: 233-235 °C; δ_H (400 MHz, DMSO) 12.13 (s, 1H, C=N-NH), 10.17 (s, 1H, S=C-NH), 10.13 (s, 1H, -OH), 9.19 (s, 1H, CH=N), 8.32 (s, 1H, -O-CH=C), 7.67 – 7.52 (m, 3H, Ar-H), 7.48 – 7.37 (m, 2H, Ar-H), 7.27 (dd, J = 9.0, 3.0 Hz, 1H, Ar-H). ^{13}C NMR (101 MHz, DMSO) δ 177.40, 175.03, 155.81, 155.74, 149.98, 139.11, 136.07, 132.19, 130.74, 129.94, 129.09, 128.13, 124.80, 123.86, 120.61, 117.49, 108.23. ESI-HRMS: m/z Formula: $C_{17}H_{11}Cl_2N_3O_3S$, calculated $[M+H]^+$: 406.98982, found $[M+H]^+$: 407.99674.

(*E*)-2-[(6-Hydroxy-4-oxo-4*H*-chromen-3-yl)methylene]-*N*-(3-methoxyphenyl)hydrazine-1-carbothioamide (4h)

Color: light-yellow; Yield: 90 %, m.p.: 227-229 °C; δ_H (400 MHz, DMSO) 11.93 (s, 1H, C=N-NH), 10.13 (s, 1H, S=C-NH), 10.06 (s, 1H, -OH), 9.28 (s, 1H, CH=N), 8.32 (s, 1H, -O-CH=C), 7.60 (d, J = 9.1 Hz, 1H, Ar-H), 7.40 (d, J = 3.0 Hz, 1H, Ar-H), 7.33 – 7.23 (m, 3H, Ar-H), 7.23 – 7.16 (s, 1H, Ar-H), 6.80 (ddd, J = 8.2, 2.6, 1.0 Hz, 1H, Ar-H), 3.78 (s, 3H, -OCH_3). ^{13}C NMR (101 MHz, DMSO) δ 176.10, 175.06, 159.52, 155.91, 155.79, 149.98, 140.53, 135.73, 129.28, 124.78, 123.85, 120.59, 118.19, 117.47, 111.75, 111.29, 108.22, 55.65. ESI-HRMS: m/z Formula: $C_{18}H_{15}N_3O_4S$, calculated $[M+H]^+$: 369.07833, found $[M+H]^+$: 370.08530.

(*E*)-2-[(6-Hydroxy-4-oxo-4*H*-chromen-3-yl)methylene]-*N*-phenethylhydrazine-1-carbothioamide (4i)

Color: white; Yield: 80 %, m.p.: 239-241 °C; δ_H (400 MHz, DMSO) 11.61 (s, 1H, C=N-NH), 10.12 (s, 1H, S=C-NH), 9.04 (s, 1H, S=C-NH), 8.65 (s, 1H, -OH), 8.21 (s, 1H, CH=N), 7.60 (d, J = 9.0 Hz, 1H, -O-CH=C), 7.39 (d, J = 3.0 Hz, 1H, Ar-H), 7.37 – 7.18 (m, 6H, Ar-H), 3.77 (ddd, J = 9.9, 7.8, 5.8 Hz, 2H, NH-CH_2), 2.98 – 2.89 (t, J = 2.1 Hz, 2H, NH-CH_2CH_2). ^{13}C NMR

(101 MHz, DMSO) δ 177.49, 175.06, 155.76, 155.06, 149.97, 139.67, 134.73, 129.05, 128.92, 126.66, 124.77, 123.83, 120.57, 117.73, 108.20, 45.48, 35.40. ESI-HRMS: m/z Formula: $C_{19}H_{17}N_3O_3S$, calculated $[M+H]^+$: 367.09906, found $[M+H]^+$: 368.10600.

(*E*)-*N*-Benzyl-2-[(6-hydroxy-4-oxo-4*H*-chromen-3-yl)methylene]hydrazine-1-carbothioamide (4j)

Color: light-yellow; Yield: 85 %, m.p.: 237-239 °C; δ_H (400 MHz, DMSO) 11.70 (s, 1H, C=N-NH), 10.11 (s, 1H, S=C-NH), 9.11 (s, 2H, -OH, CH=N), 8.24 (s, 1H, -O-CH=C), 7.57 (d, J = 9.0 Hz, 1H, Ar-H), 7.38 (d, J = 3.0 Hz, 1H, Ar-H), 7.38 – 7.25 (m, 4H, Ar-H), 7.26 (dd, J = 9.0, 3.0 Hz, 2H, Ar-H), 4.86 (d, J = 6.4 Hz, 2H, CH_2-Ar). ^{13}C NMR (101 MHz, DMSO) δ 178.14, 175.05, 155.75, 155.30, 149.97, 139.77, 135.00, 128.66, 127.63, 127.23, 124.77, 123.81, 120.55, 117.68, 108.20, 47.01. ESI-HRMS: m/z Formula: $C_{18}H_{15}N_3O_3S$, calculated $[M+H]^+$: 353.08341, found $[M+H]^+$: 354.09039.

(*E*)-*N*-(2,6-Dichlorophenyl)-2-[(6-hydroxy-4-oxo-4*H*-chromen-3yl)methylene]hydrazine-1-carbothioamide (4k)

Color: white; Yield: 86 %, m.p.: 237-239 °C; δ_H (400 MHz, DMSO) 12.10 (s, 1H, 1H, C=N-NH), 10.13 (s, 1H, S=C-NH), 10.10 (s, 1H, -OH), 9.22 (s, 1H, CH=N), 8.31 (s, 1H, -O-CH=C), 7.71 – 7.50 (m, 3H, Ar-H), 7.48 – 7.34 (m, 2H, Ar-H), 7.27 (dd, J = 9.0, 3.0 Hz, 1H, Ar-H). ^{13}C NMR (101 MHz, DMSO) δ 177.75, 175.05, 155.78, 155.70, 150.01, 135.76, 135.69, 135.34, 129.96, 128.85, 124.82, 123.83, 120.62, 117.51, 108.23. ESI-HRMS: m/z Formula: $C_{17}H_{11}Cl_2N_3O_3S$, calculated $[M+H]^+$: 406.98982, found $[M+H]^+$: 407.99687.

(*E*)-2-[(6-Hydroxy-4-oxo-4*H*-chromen-3-yl)methylene]-*N*-isobutylhydrazine-1-carbothioamide (4l)

Color: white; Yield: 89 %, m.p.: 226-228 °C; δ_H (400 MHz, DMSO) 11.53 (s, 1H, C=N-NH), 10.10 (s, 1H, S=C-NH), 9.10 (s, 1H, -OH), 8.53 (s, 1H, CH=N), 8.20 (s, 1H, -O-CH=C), 7.58 (d, J = 9.0 Hz, 1H, Ar-H), 7.38 (d, J = 3.0 Hz, 1H, Ar-H), 7.26 (dd, J = 9.0, 3.0 Hz, 1H, Ar-H), 3.40 (t, J = 6.5 Hz, 2H, NH-CH_2), 2.02 (dt, J = 13.5, 6.8 Hz, 1H, $CH(CH_3)_2$), 0.90 (d, J = 6.7 Hz, 6H, $CH(CH_3)_2$). ^{13}C NMR (101 MHz, DMSO) δ 177.76, 175.05, 155.73, 155.22, 149.96, 134.61, 124.77, 123.80, 120.54, 117.72, 108.20, 51.31,

28.36, 20.60. ESI-HRMS: m/z Formula: $C_{15}H_{17}N_3O_3S$, calculated $[M+H]^+$: 319.09906, found $[M+H]^+$: 320.10623.

(*E*)-*N*-(4-Bromo-2-fluorophenyl)-2-[(6-hydroxy-4-oxo-4*H*-chromen-3-yl)methylene]hydrazine-1-carbothioamide (4m)

Color: light-yellow; Yield: 85 %, m.p.: 243-245 °C; δ_H (400 MHz, DMSO) 12.13 (s, 1H, C=N-NH), 10.14 (s, 1H, S=C-NH), 9.97 (s, 1H, -OH), 9.20 (s, 1H, CH=N), 8.31 (s, 1H, -O-CH=C), 7.68 – 7.62 (m, 1H, Ar-H), 7.59 (d, J = 9.1 Hz, 1H, Ar-H), 7.46 (dd, J = 3.8, 1.6 Hz, 2H, Ar-H), 7.40 (d, J = 3.0 Hz, 1H, Ar-H), 7.27 (dd, J = 9.0, 3.0 Hz, 1H, Ar-H). ^{13}C NMR (101 MHz, DMSO) δ 177.75, 175.03, 155.81, 149.98, 136.20, 132.45, 127.78, 127.74, 127.25, 127.13, 124.80, 123.87, 120.61, 119.80, 119.56, 117.46, 108.23. ESI-HRMS: m/z Formula: $C_{17}H_{11}FBrN_3O_3S$, calculated $[M+H]^+$: 434.96885, found $[M+H]^+$: 437.97393

(*E*)-*N*-(2,4-Dimethylphenyl)-2-[(6-hydroxy-4-oxo-4*H*-chromen-3-yl)methylene]hydrazine-1-carbothioamide (4n)

Color: white; Yield: 90 %, m.p.: 238-240 °C; δ_H (400 MHz, DMSO) 11.90 – 11.68 (m, 1H, C=N-NH), 10.12 (s, 1H, S=C-NH), 9.89 (s, 1H, -OH), 9.24 (s, 1H, CH=N), 8.29 (s, 1H, -O-CH=C), 7.58 (d, J = 9.0 Hz, 1H, Ar-H), 7.40 (d, J = 3.1 Hz, 1H, Ar-H), 7.26 (dd, J = 9.0, 3.1 Hz, 1H, Ar-H), 7.13 (d, *J* = 7.9 Hz, 1H, Ar-H), 7.08 (s, 1H, Ar-H), 7.03 (s, 1H, Ar-H), 2.30 (s, 3H, -CH_3), 2.19 (s, 3H, -CH_3). ^{13}C NMR (101 MHz, DMSO) δ 177.47, 175.06, 155.75, 155.69, 149.99, 136.40, 135.81, 135.71, 135.03, 131.12, 129.06, 126.96, 124.80, 123.81, 120.58, 117.65, 108.21, 21.09, 18.22. ESI-HRMS: m/z Formula: $C_{19}H_{17}N_3O_3S$, calculated $[M+H]^+$: 367.09906, found $[M+H]^+$: 368.10612.

(*E*)-2-[(6-Hydroxy-4-oxo-4*H*-chromen-3-yl)methylene]hydrazine-1-carbothioamide (4o)

Color: yellow; Yield: 84 %, m.p.: 249-251 °C; δ_H 1H NMR (400 MHz, DMSO) δ 11.52 (s, 1H, C=N-NH), 10.12 (s, 1H, S=C-NH), 9.1 (s, 1H, -OH), 8.22 (d, *J* = 12.4 Hz, 2H, Ar-H), 8.07 (s, 1H, Ar-H), 7.59 (d, *J* = 9.0 Hz, 1H, Ar-H), 7.38 (d, *J* = 3.0 Hz, 1H, Ar-H), 7.26 (dd, *J* = 9.0, 3.1 Hz, 1H, Ar-H). ^{13}C NMR (101 MHz, DMSO) δ 178.50, 175.06, 155.72, 155.36, 149.96, 134.97,

124.75, 123.80, 120.55, 117.67, 108.17. ESI-HRMS: m/z Formula: $C_{11}H_9N_3O_3S$, calculated $[M+H]^+$: 263.03646, found $[M+H]^+$: 264.04373.

(*E*)-*N*-(4-Chlorobenyl)-2-[(6-hydroxy-4-oxo-4*H*-chromen-3-yl)methylene]hydrazine-1-carbothioamide (4p)

Color: light-yellow; Yield: 90 %, m.p.: 260-262 °C; δ_H (400 MHz, DMSO) 11.73 (s, 1H, C=N-NH), 10.11 (s, 1H, S=C-NH), 9.11 (s, 1H, -OH), 9.09 (s, 1H, CH=N), 8.24 (s, 1H, O-CH=C), 7.58 (d, J = 9.1 Hz, 1H, Ar-H), 7.46 – 7.33 (m, 5H, Ar-H), 7.26 (dd, J = 9.1, 3.1Hz, 1H, Ar-H), 4.83 (d, J = 6.2 Hz, 2H, N-CH_2-Ar). ^{13}C NMR (101 MHz, DMSO) δ 178.18, 175.05, 155.76, 155.28, 149.97, 138.85, 135.14, 131.76, 129.52, 128.61, 124.77, 123.82, 120.56, 117.66, 108.21, 46.34. ESI-HRMS: m/z Formula: $C_{18}H_{14}ClN_3O_3S$, calculated $[M+H]^+$: 387.04444, found $[M+H]^+$: 388.05154.

3.4. *In-silico* Studies

BioSolveIT's LeadIT software[58, 59] was employed to carry out molecular docking studies. Since all compounds **4(a-p)** were excellent inhibitors of both enzymes' α-Glucosidase and α-Amylase, all compounds were docked against these two enzymes.[50, 52] A total of 10 docked conformations were produced for each compound; the docked pose having the best docking score was detailed visualization of binding site interactions. Desmond Molecular Dynamics (D.E. Shaw Research) software using the Schrödinger Maestro 2024.4 program was used for the study of Molecular Dynamics Simulation of inhibitor-protein complexes.[60] The best docked pose of **4g**-α-Amylase was used for the starting reference structure. Maestro's protein preparation module was used for pre-processing and refinement of the complex structure. Solvation was done through the system builder module, and the pre-determined solvent model TIP3P[60] with an orthorhombic box shape was opted for solvation with 10 Å x 10 Å x 10 Å buffer dimensions. Ions distribution was done using default values determined by the software; additionally, 0.15M NaCl was also used for the simulation of natural physiological conditions.[60] In the MD panel, a 100ns (nanoseconds) simulation time was set, as well as the trajectory recording interval was 100ps (picoseconds), resulting in approximately 1000 frames. The system was operated using the default relaxation technique, NPT ensemble at

1.01325 bar pressure and 300K temperature using Martyna-Tobias-Klein barostat and Nosé-Hoover chain thermostat settings.[60] Simulations, the Interaction Diagram panel, and trajectory analysis were used for results analysis in Maestro.[60]

3.5. Network Pharmacology

To elucidate the molecular mechanisms underlying the antidiabetic and antioxidant potential of the synthesized compounds, a network pharmacology-based analysis was performed. Initially, the potential targets of the studied compounds were predicted using the DIGEP-Pred server [61], which identifies genes modulated by small molecules based on transcriptional response profiles. Targets with a probability score greater than 0.5 were considered significant, yielding a total of 65 genes. In parallel, GeneCards database analysis [62] was carried out to identify genes associated with diabetes and antioxidant properties. For this purpose, the search terms “diabetes” and “antioxidant” were independently queried, and genes with a GeneCards relevance (GIFt) score [63] above 65 were selected, resulting in 181 candidate genes. Subsequently, Venn diagram analysis [64] was performed to determine the overlap between compound-associated genes (from DIGEP-Pred) and disease-associated genes (from GeneCards). The intersection revealed 11 common genes, indicating shared molecular targets between the compound activity and diabetes-related oxidative stress pathways. To further delineate the biological relevance of these targets, KEGG pathway enrichment analysis was performed using the KEGG Mapper tool [65], where identified genes were mapped to metabolic and signaling pathways associated with diabetes and oxidative regulation. Additionally, Gene Ontology (GO) enrichment analysis [66a,b] is performed to categorize the shared targets based on biological processes, molecular functions, and cellular components, thereby providing insight into their physiological roles in antioxidant regulation and diabetes progression.

3.6. Post Molecular Dynamics Simulation Analyses

3.6.1 PCA and DCCM Analyses

Dynamic cross-correlation matrix (DCCM) and Principal Component Analysis (PCA) analyses of the simulations of both complexes were carried out using the Bio3D package version 2.4.5 [67] in R programming environment version 4.5.1 . VMD (Visual Molecular Dynamics) program version 2.0.0a4 was used to get the topology and trajectory format acceptable for Bio3D.

3.6.2 Free Energy Landscape Analysis

Radius of Gyration - Root Mean Square Deviation (RG-RMSD) based method for Free Energy Landscape (FEL) analysis of the simulations was performed to assess the energy and stability of the complexes using Geo Measures v0.9d [68] plugin in PyMol version 3.1.0 open-source build.

3.7. In vitro biological assays

3.7.1 Assay for DPPH Radical Scavenging

A spectrophotometric technique was used to measure the DPPH (2,2-diphenyl-1-picrylhydrazyl) radical scavenging activity. DPPH powder was dissolved in ethanol to create a freshly made DPPH solution (0.1 mM), which was then shielded from light before usage.[69] To achieve the required concentrations, test substances were first dissolved in dimethyl sulfoxide (DMSO) and then diluted with ethanol, making sure that the final DMSO level did not surpass 1% (v/v). The reference antioxidant was Trolox. In a 96-well plate, 100 µL of the test drug solution and 100 µL of the DPPH solution were combined for the experiment. To enable radical scavenging, the reaction mixture was incubated for 30 minutes at room temperature in the dark. A microplate reader was used to measure the absorbance reduction at 517 nm. IC_{50} values were derived using concentration–response curves, and the radical scavenging activity was computed in relation to the control.[70]

3.7.2 Assay for ABTS Radical Scavenging

A colorimetric approach was used to assess the ABTS [2,2-azinobis(3-ethylbenzothiazoline-6-sulfonic acid)] radical cation scavenging activity. A

7 mM ABTS stock solution was reacted with 2.45 mM potassium persulfate to produce the $ABTS^{\bullet+}$ radical cation.[71] The mixture was then left at room temperature in the dark for 12–16 hours. The $ABTS^{\bullet+}$ solution was diluted with ethanol or phosphate-buffered saline before to the experiment in order to achieve an absorbance of 0.75 ± 0.05 at 734 nm. In order to keep the final DMSO concentration below 1%, test compounds were dissolved in DMSO and diluted using the same solvent employed for $ABTS^{\bullet+}$ dilution. During the assay process, 100 µL of the diluted $ABTS^{\bullet+}$ solution was mixed with 100 µL of the test chemical solution. After six minutes of room temperature incubation, the reaction mixture's absorbance decrease was measured at 734 nm. The typical antioxidant used was trolox. IC_{50} values were obtained and was computed.[72]

Additionally, for antioxidant assays, IC_{50} values were determined by plotting concentration versus percentage radical scavenging activity in Microsoft Excel. Using the MAVS approach, exponential trendlines were generated for each sample by selecting the exponential fitting option, and the control absorbance was entered as the cutoff value. The resulting equations were used to calculate IC_{50} values individually through logarithmic transformation. All experiments were performed in triplicate, and the results are expressed as mean ± standard deviation.

3.7.3 Assay for α-Glucosidase Inhibition

A slightly modified spectrophotometric approach was used to determine the α-Glucosidase inhibitory activity. *Saccharomyces cerevisiae*'s α-Glucosidase enzyme was dissolved in 0.1 M phosphate buffer (pH 6.8) to achieve a final activity of 0.5 U/mL. P-nitrophenyl-α-D-glucopyranoside (pNPG), the substrate solution, was made fresh in the same phosphate buffer at a concentration of 5 mM. To reach the required concentrations, test substances were dissolved in dimethyl sulfoxide (DMSO) and then further diluted using phosphate buffer, making sure that the final DMSO content did not surpass 1% (v/v).[73] In short, 50 µL of the enzyme solution and 50 µL of the test chemical solution were combined, and the mixture was pre-incubated for 10 minutes at 37 °C. The reaction was then started by adding 50 µL of the p-NPG substrate solution. After 20 more minutes of

incubation at 37 °C, the reaction mixture was stopped by adding 100 µL of 0.2 M Na_2CO_3. Spectrophotometric measurements of the p-nitrophenol release were made at 405 nm. The reference inhibitor was acarbose. IC_{50} values were calculated and was compared to the control.[74]

3.7.4 Assay for α-Amylase Inhibition

A colorimetric approach was used to assess the A-amylase inhibitory activity. The porcine pancreas α-Amylase enzyme was dissolved in 20 mM phosphate buffer (pH 6.9) with 6.7 mM NaCl to provide an enzyme solution with a final concentration of 1 U/mL.[75] The substrate was soluble starch, which was freshly made as a 1% (w/v) solution in the same buffer by slowly heating it until it completely dissolved. In order to keep the final DMSO concentration below 1%, test chemicals were first dissolved in DMSO and then diluted with phosphate buffer to the necessary concentrations. 50 µL of α-Amylase solution and 50 µL of the test chemical were combined and pre-incubated for 10 minutes at 37 °C. The enzymatic reaction was then initiated by adding 50 µL of the starch solution, and it was then incubated for 15 minutes at 37 °C. After adding 100 µL of dinitrosalicylic acid (DNS) reagent to halt the reaction, the mixture was heated to 100 °C for five minutes to produce color. Absorbance was measured at 540 nm after cooling to ambient temperature. The typical inhibitor was acarbose. In accordance with this, IC_{50} values inhibition were computed.[76]

For enzyme inhibition assays, IC_{50} values were calculated using mathematical formulas based on concentration–response relationships. The calculations considered the molecular weights of the tested compounds and the dilution factors applied in the solvent to ensure accurate concentration values. Percentage inhibition was determined for each concentration, and dose response curves were generated using Microsoft Excel. The IC_{50} values were obtained from the logarithmic regression equation by dividing 0.693 by the coefficient corresponding to the concentration term (x) in the fitted equation.

4. Conclusion

In conclusion, a series 6-hydroxychromone-based thiosemicarbazones were synthesized and evaluated for α-Glucosidase and α-Amylase inhibition and anti-oxidant activity. These synthesized compounds exhibited moderate to strong inhibitory potencies, with **4k** and **4g** demonstrated the most effective inhibition against α-Glucosidase and α-Amylase, respectively, outperforming the standard drug Acarbose. Compounds **4o** and **4g** showed promising DPH and ABTS radical scavenging activity. MD simulation (RMSD <3.6 Å, low RMSF (<2.8 Å)) and docking confirmed their interaction with binding sites. The network pharmacology analysis revealed significant involvement of these compounds in regulating key targets and pathways, thereby modulating diabetic and oxidative stress. Collectively, these outcomes emphasize the significance of this pharmacophore as a key candidate for designing next-generation agents with anti-diabetic and antioxidant activities, warranting further preclinical studies to evaluate their pharmacokinetic properties and therapeutic efficacy.

CRediT authorship contribution statement

Wajeeha Zareen, Farhan Siddique: Investigation, Formal analysis. **Nadeem Ahmed**: Writing – original draft, Validation. **Mostafa A. Ismail, Rima D. Alharthy:** Formal analysis, software, Funding acquisition. **Parham Taslimi, Mariya al-Rashida, Talha Islam:** Formal analysis, software, Data curation, Investigation. Supervision, Conceptualization. **Magdi E. A. Zaki, Sobhi M. Gomha:** Formal analysis, Data curation, Funding acquisition. **Zahid Shafiq, Ali Muhamad Khan**: Writing – original draft, Supervision, Conceptualization.

Acknowledgment

The authors express their appreciation to the Deanship of Scientific Research at King Khalid University, Saudi Arabia, for this work through Large Research Project under grant number RGP2/684/46.

Data availability

All data generated or analyzed during this study are included in this published article [and its supplementary information files.

Funding Declaration:

The authors express their appreciation to the Deanship of Scientific Research at King Khalid University, Saudi Arabia, for this work through Large Research Project under grant number RGP2/684/46.

References

(1) Cheng, X.; Huang, J.; Li, H.; Zhao, D.; Liu, Z.; Zhu, L.; Zhang, Z.; Peng, W. Quercetin: A promising therapy for diabetic encephalopathy through inhibition of hippocampal ferroptosis. *Phytomedicine* **2024**, *126*, 154887.
(2) Su, M.; Tang, T.; Tang, W.; Long, Y.; Wang, L.; Liu, M. Astragalus improves intestinal barrier function and immunity by acting on intestinal microbiota to treat T2DM: a research review. *Frontiers in Immunology* **2023**, *Volume 14 - 2023*, Review. DOI: 10.3389/fimmu.2023.1243834.
(3) Li, M.; Li, H.; Min, X.; Sun, J.; Liang, B.; Xu, L.; Li, J.; Wang, S.-H.; Xu, X. Identification of 1,3,4-Thiadiazolyl-Containing Thiazolidine-2,4-dione Derivatives as Novel PTP1B Inhibitors with Antidiabetic Activity. *Journal of Medicinal Chemistry* **2024**, *67* (10), 8406-8419.
(4) Shao, D.-W.; Zhao, L.-J.; Sun, J.-F. Synthesis and clinical application of representative small-molecule dipeptidyl Peptidase-4 (DPP-4) inhibitors for the treatment of type 2 diabetes mellitus (T2DM). *European Journal of Medicinal Chemistry* **2024**, *272*, 116464.
(5) Zhou, Y.; Liu, L.; Xiang, R.; Bu, X.; Qin, G.; Dai, J.; Zhao, Z.; Fang, X.; Yang, S.; Han, J. Arctigenin mitigates insulin resistance by modulating the IRS2/GLUT4 pathway via TLR4 in type 2 diabetes mellitus mice. *International immunopharmacology* **2023**, *114*, 109529.
(6) Mi, W.; Xia, Y.; Bian, Y. The influence of ICAM1 rs5498 on diabetes mellitus risk: evidence from a meta-analysis. *Inflamm Res* **2019**, *68* (4), 275-284.
(7) Kaur, N.; Kumar, V.; Nayak, S. K.; Wadhwa, P.; Kaur, P.; Sahu, S. K. Alpha-amylase as molecular target for treatment of diabetes mellitus: A comprehensive review. *Chemical biology & drug design* **2021**, *98* (4), 539-560.
(8) Hameed, S.; Khan, K. M.; Salar, U.; Özil, M.; Baltaş, N.; Saleem, F.; Qureshi, U.; Taha, M.; Ul-Haq, Z. Hydrazinyl thiazole linked indenoquinoxaline hybrids: Potential leads to treat hyperglycemia and oxidative stress; Multistep synthesis, α-Amylase, α-glucosidase inhibitory and antioxidant activities. *International Journal of Biological Macromolecules* **2022**, *221*, 1294-1312.
(9) Apaydın, Ç. B.; Celikok, G. H.; Özden, T. Y.; Cihan-üstündağ, G. Design, synthesis and biological evaluation of novel sulfonamide hydrazones as α-glucosidase and α-Amylase inhibitors. *istanbul Journal of Pharmacy* **2022**, *52* (2), 108-113.
(10) Peng, Q.; Zhang, H.; Li, Z. Methyltransferase-like 16 drives diabetic nephropathy progression via epigenetic suppression of V-set pre-B cell surrogate light chain 3. *Life Sci* **2025**, *374*, 123694. DOI: 10.1016/j.lfs.2025.123694 From NLM.
(11) Chen, X.; Chen, C.; Tian, X.; He, L.; Zuo, E.; Liu, P.; Xue, Y.; Yang, J.; Chen, C.; Lv, X. DBAN: An improved dual branch attention network combined with serum Raman spectroscopy for diagnosis of diabetic kidney disease. *Talanta* **2024**, *266* (Pt 2), 125052.
(12) Mokoena, T. P.; Maluleka, M. M.; Mampa, R. M.; Mphahlele, M. J.; Monchusi, B. A. Synthesis, crystal structures, spectroscopic characterization and in vitro evaluation of the 4-sulfono-3-methoxycinnamaldehydes as potential α-glucosidase and/or α-Amylase inhibitors. *Journal of Molecular Structure* **2023**, *1271*, 134119.
(13) Rafique, R.; Khan, K. M.; Chigurupati, S.; Wadood, A.; Rehman, A. U.; Karunanidhi, A.; Hameed, S.; Taha, M.; Al-Rashida, M. Synthesis of new indazole based dual inhibitors of α-Glucosidase and α-Amylase enzymes, their in vitro, in silico and kinetics studies. *Bioorganic chemistry* **2020**, *94*, 103195.
(14) Assila, H.; Brandan, S. A.; Mortada, S.; Zaoui, Y.; Alzahrani, A. Y. A.; Arshad, S.; Ramli, Y.; Faouzi, M. E. A.; Karrouchi, K.; Ansar, M. h. Pyridazine derivative as potent

antihyperglycemic agent: Synthesis, crystal structure, α-Amylase and α-Glucosidase inhibition and computational studies. *Journal of Molecular Structure* **2024**, *1308*, 138145.
(15) Ullah, W.; Rahim, F.; Hayat, S.; Ullah, H.; Taha, M.; Khan, S.; Khaliq, A.; Bibi, S.; Gohar, O.; Iqbal, N. Synthesis of indole based sulfonamide derivatives as potent inhibitors of α-Glucosidase and α-Amylase in management of type-II diabetes. *Chemical Data Collections* **2024**, *50*, 101122.
(16) Cakmak, U.; Oz-Tuncay, F.; Basoglu-Ozdemir, S.; Ayazoglu-Demir, E.; Demir, I.; Colak, A.; Celik-Uzuner, S.; Erdem, S. S.; Yildirim, N. Synthesis of hydrazine containing piperazine or benzimidazole derivatives and their potential as α-Amylase inhibitors by molecular docking, inhibition kinetics and in vitro cytotoxicity activity studies. *Medicinal Chemistry Research* **2021**, *30* (10), 1886-1904.
(17) Noreen, T.; Taha, M.; Imran, S.; Chigurupati, S.; Rahim, F.; Selvaraj, M.; Ismail, N. H.; Mohammad, J. I.; Ullah, H.; Nawaz, F. Synthesis of α-Amylase inhibitors based on privileged indole scaffold. *Bioorganic chemistry* **2017**, *72*, 248-255.
(18) Naseer, I.; Tariq, H. Z.; Siddique, F.; Sadeghian, N.; Nadeem, S.; Wajid, M.; Taslimi, P.; Alanazi, A. K.; Batool, Z.; Li, J. Synthesis, Antidiabetic Assessment, Metal Chelating Impacts, and Computational Modeling of 4-Fluorophenyl sulfonyl-indole Based Hydrazones. *Journal of Molecular Structure* **2025**, 143878.
(19) Saleem, F.; Khan, K. M.; Ullah, N.; Özil, M.; Baltaş, N.; Hameed, S.; Salar, U.; Wadood, A.; Rehman, A. U.; Kumar, M. Bioevaluation of synthetic pyridones as dual inhibitors of α-amylase and α-glucosidase enzymes and potential antioxidants. *Archiv der Pharmazie* **2023**, *356* (1), 2200400.
(20) Oladipo, S. D.; Luckay, R. C.; Olofinsan, K. A. Evaluating the antidiabetes and antioxidant activities of halogenated Schiff bases derived from 4-(diethylamino) salicylaldehyde: in vitro antidiabetes, antioxidant and computational investigation. *Scientific Reports* **2024**, *14* (1), 27073.
(21) Vallabhaneni, M. R.; Nathani, S. R.; Kondraganti, L.; Addanki, H. R.; Bodepudi, S. C. Antidiabetic and antioxidant activities of synthetic 2-styrylchromones. *Bioorganic & Medicinal Chemistry Reports* **2025**, *8* (1).
(22) Yadav, P.; Sharma, S.; Kumari, S.; Ranka, M. Green synthesis and biological significance of chromone derivatives with amino acid and their metal complexes as antimicrobial, anti-diabetic and anti-oxidant. *Journal of the Indian Chemical Society* **2024**, *101* (10), 101263.
(23) AlNeyadi, S. S.; Amer, N.; Thomas, T. G.; Ajeil, R. A.; Breitener, P.; Munawar, N. Synthesis, characterization, and antioxidant activity of some 2-methoxyphenols derivatives. *Heterocyclic Communications* **2020**, *26* (1), 112-122.
(24) Saif, M. Z.; Esha, N. J. I.; Quayum, S. T.; Rahman, S.; Al-Gawati, M. A.; Alsowygh, G.; Albrithen, H.; Alodhayb, A. N.; Poirier, R. A.; Uddin, K. M. Investigating the potential of 6-substituted 3-formyl chromone derivatives as anti-diabetic agents using in silico methods. *Scientific Reports* **2024**, *14* (1), 13221.
(25) Auti, P. S.; Jagetiya, S.; Paul, A. T. Chromone containing hybrid analogs: Synthesis and applications in medicinal chemistry. *Chemistry & Biodiversity* **2023**, *20* (8), e202300587.
(26) Fan, M.; Yang, W.; Peng, Z.; He, Y.; Wang, G. Chromone-based benzohydrazide derivatives as potential α-glucosidase inhibitor: Synthesis, biological evaluation and molecular docking study. *Bioorganic Chemistry* **2023**, *131*, 106276.
(27) Costa, M.; Dias, T. A.; Brito, A.; Proença, F. Biological importance of structurally diversified chromenes. *European Journal of Medicinal Chemistry* **2016**, *123*, 487-507.
(28) Kini, J. H.; Pai, V. K.; Bodke, Y. D. Design and Synthesis of Some Chromone derivatives of biological importance: A Greener Approach. *Materials Today: Proceedings* **2017**, *4* (11, Part 3), 11894-11901.
(29) Kaishap, P. P.; Laskar, B.; Dutta, D.; Gogoi, N.; Dey, T. Harnessing Chromone as a Versatile Scaffold for Emerging Biological Applications: Recent Advances and Medicinal Insights. *Chem Rec* **2025**, *25* (11), e202500073. DOI: 10.1002/tcr.202500073 From NLM.
(30) Keri, R. S.; Budagumpi, S.; Pai, R. K.; Balakrishna, R. G. Chromones as a privileged scaffold in drug discovery: A review. *European Journal of Medicinal Chemistry* **2014**, *78*, 340-374.
(31) Garbuz, O.; Ceban, E.; Istrati, D.; Railean, N.; Toderas, I.; Gulea, A. Thiosemicarbazone-Based Compounds: Cancer Cell Inhibitors with Antioxidant Properties. *Molecules* **2025**, *30* (9), 2077.

(32) Zahra, S. B.; Khan, A.; Ahmed, N.; Rafique, M.; Fatima, L.; Khan, I.; Hussain, J.; Khalid, S.; Ogaly, H. A.; Ahmed, M. M.; et al. Versatile biological activities of thiosemicarbazones and their metal complexes. *Journal of Molecular Structure* **2025**, *1322*, 140511.
(33) Sever, B.; Soybir, H.; Görgülü, Ş.; Cantürk, Z.; Altıntop, M. D. Pyrazole incorporated new thiosemicarbazones: Design, synthesis and investigation of DPP-4 inhibitory effects. *Molecules* **2020**, *25* (21), 5003.
(34) Imran, A.; Shehzad, M. T.; Shah, S. J. A.; Al Adhami, T.; Laws, M.; Rahman, K. M.; Alharthy, R. D.; Khan, I. A.; Shafiq, Z.; Iqbal, J. Development and exploration of novel substituted thiosemicarbazones as inhibitors of aldose reductase via in vitro analysis and computational study. *Scientific Reports* **2022**, *12* (1), 5734.
(35) Maicheen, C.; Churnthammakarn, C.; Pongsroypech, N.; Khamkhenshorngphanuch, T.; Ungwitayatorn, J.; Rungsardthong, K.; Asasutjarit, R.; Theeramunkong, S. One-Pot Synthesis and Evaluation of Antioxidative Stress and Anticancer Properties of an Active Chromone Derivative. *Molecules* **2023**, *28* (7), 3129.
(36) Wang, G.; Chen, M.; Wang, J.; Peng, Y.; Li, L.; Xie, Z.; Deng, B.; Chen, S.; Li, W. Synthesis, biological evaluation and molecular docking studies of chromone hydrazone derivatives as α-glucosidase inhibitors. *Bioorganic & Medicinal Chemistry Letters* **2017**, *27* (13), 2957-2961.
(37) Santos, C. M.; Proença, C.; Freitas, M.; Araújo, A. N.; Silva, A. M.; Fernandes, E. 2-Styrylchromones as inhibitors of α-Amylase and α-Glucosidase enzymes for the management of type 2 diabetes mellitus. *Medicinal Chemistry Research* **2024**, *33* (4), 600-610.
(38) Elmsellem, H.; Elyoussfi, A.; Steli, H.; Sebbar, N.; Essassi, E.; Dahmani, M.; El Ouadi, Y.; Aouniti, A.; El Mahi, B.; Hammouti, B. The theobromine (chocolate) as green inhibitor of mild steel corrosion in hydrochloric acid: Electrochemical and theoretical quantum studies. *Der Pharma Chemica* **2016**, *8* (1), 248-256.
(39) Jorepalli, S.; Adikay, S.; Chinthaparthi, R. R.; Gangireddy, C. S. R.; Koduru, J. R.; Karri, R. R. Synthesis, molecular docking studies and biological evaluation of N-(4-oxo-2-(trifluoromethyl)-4 H-chromen-7-yl) benzamides as potential antioxidant, and anticancer agents. *Scientific Reports* **2024**, *14* (1), 9866.
(40) Czylkowska, A.; Pitucha, M.; Raducka, A.; Fornal, E.; Kordialik-Bogacka, E.; Ścieszka, S.; Smoluch, M.; Burdan, F.; Jędrzejec, M.; Szymański, P. Thiosemicarbazone-Based Compounds: A Promising Scaffold for Developing Antibacterial, Antioxidant, and Anticancer Therapeutics. *Molecules* **2024**, *30* (1), 129.
(41) Pitucha, M.; Ramos, P.; Wojtunik-Kulesza, K.; Głogowska, A.; Stefańska, J.; Kowalczuk, D.; Monika, D.; Augustynowicz-Kopeć, E. Thermal analysis, antimicrobial and antioxidant studies of thiosemicarbazone derivatives. *Journal of Thermal Analysis and Calorimetry* **2023**, *148* (10), 4223-4234.
(42) Tok, F.; Küçükal, B.; Baltaş, N.; Tatar Yılmaz, G.; Koçyiğit-Kaymakçıoğlu, B. Synthesis of novel thiosemicarbazone derivatives as antidiabetic agent with enzyme kinetic studies and antioxidant activity. *Phosphorus, Sulfur, and Silicon and the Related Elements* **2022**, *197* (12), 1284-1294.
(43) Ullah, H.; Khan, S.; Rahim, F.; Taha, M.; Iqbal, R.; Sarfraz, M.; Shah, S. A. A.; Sajid, M.; Awad, M. F.; Omran, A. Benzimidazole bearing thiosemicarbazone derivatives act as potent α-Amylase and α-Glucosidase inhibitors; synthesis, bioactivity screening and molecular docking study. *Molecules* **2022**, *27* (20), 6921.
(44) Shoukat, W.; Hussain, M.; Ali, A.; Shafiq, N.; Chughtai, A. H.; Shakoor, B.; Moveed, A.; Shoukat, M. N.; Milošević, M.; Mohany, M. Design, synthesis, characterization and biological screening of novel thiosemicarbazones and their derivatives with potent antibacterial and antidiabetic activities. *Journal of Molecular Structure* **2025**, *1320*, 139614.
(45) Thanh, N. D.; Hoai le, T. Synthesis, Structure and Antioxidant Activity of (Tetra-O-acetyl-β-D-galactopyranosyl)thiosemicarbazones of Substituted Benzaldehydes. *Indian J Pharm Sci* **2012**, *74* (1), 54-62. DOI: 10.4103/0250-474x.102544 From NLM.
(46) Sens, L.; Oliveira, A. S. d.; Mascarello, A.; Brighente, I. M. C.; Yunes, R. A.; Nunes, R. J. Synthesis, Antioxidant Activity, Acetylcholinesterase Inhibition and Quantum Studies of Thiosemicarbazones. *Journal of the Brazilian Chemical Society* **2017**, *29*, 343-352.
(47) Yang, L.; Liu, H.; Xia, D.; Wang, S. Antioxidant Properties of Camphene-Based Thiosemicarbazones: Experimental and Theoretical Evaluation. *Molecules* **2020**, *25* (5). DOI: 10.3390/molecules25051192 From NLM.

(48) Muğlu, H. Synthesis, spectroscopic characterization, DFT studies and antioxidant activity of new 5-substituted isatin/thiosemicarbazones. *Journal of Molecular Structure* **2025**, *1322*, 140406.
(49) Czylkowska, A.; Pitucha, M.; Raducka, A.; Fornal, E.; Kordialik-Bogacka, E.; Ścieszka, S.; Smoluch, M.; Burdan, F.; Jędrzejec, M.; Szymański, P. Thiosemicarbazone-Based Compounds: A Promising Scaffold for Developing Antibacterial, Antioxidant, and Anticancer Therapeutics. *Molecules* **2025**, *30* (1), 129.
(50) Chaudhry, F.; Naureen, S.; Huma, R.; Shaukat, A.; Al-Rashida, M.; Asif, N.; Ashraf, M.; Munawar, M. A.; Khan, M. A. In search of new α-glucosidase inhibitors: Imidazolylpyrazole derivatives. *Bioorganic chemistry* **2017**, *71*, 102-109.
(51) Wang, S.; Yang, C.; Chen, L. LSA-DDI: Learning Stereochemistry-Aware Drug Interactions via 3D Feature Fusion and Contrastive Cross-Attention. *International Journal of Molecular Sciences* **2025**, *26* (14), 6799.
(52) Williams, L. K.; Zhang, X.; Caner, S.; Tysoe, C.; Nguyen, N. T.; Wicki, J.; Williams, D. E.; Coleman, J.; McNeill, J. H.; Yuen, V. The amylase inhibitor montbretin A reveals a new glycosidase inhibition motif. *Nature chemical biology* **2015**, *11* (9), 691-696.
(53) Wang, K.; Yin, J.; Chen, J.; Ma, J.; Si, H.; Xia, D. Inhibition of inflammation by berberine: Molecular mechanism and network pharmacology analysis. *Phytomedicine* **2024**, *128*, 155258. DOI: 10.1016/j.phymed.2023.155258 From NLM.
(54) Zhou, C.; Yu, Z.; Chen, T.; Chen, Q.; Zhang, Y.; Cai, J.; Xu, C.; Yu, L. Tanshinone IIA attenuates cerebral-ischemia-reperfusion-induced neuroinflammation by inhibiting the TLR4/NF-κB signaling cascade: A study integrating network pharmacology, bioinformatics, and experimental validation. *Phytomedicine* **2025**, *149*, 157548.
(55) Li, W.; Yuan, G.; Pan, Y.; Wang, C.; Chen, H. Network pharmacology studies on the bioactive compounds and action mechanisms of natural products for the treatment of diabetes mellitus: A review. *Frontiers in Pharmacology* **2017**, *8*, 74.
(56) Sun, X.; Ji, Y.; Tahir, A.; Kang, J. Network pharmacology combined with transcriptional analysis to unveil the biological basis of astaxanthin in reducing the oxidative stress induced by diabetes mellitus. *Diabetes, Metabolic Syndrome and Obesity* **2020**, 4281-4295.
(57) Alharthy, R. D.; Khalid, S.; Fatima, S.; Ullah, S.; Khan, A.; Mali, S. N.; Jawarkar, R. D.; Dhabarde, S. S.; Kashtoh, H.; Taslimi, P.; et al. Synthesis of the chromone-thiosemicarbazone scaffold as promising α-glucosidase inhibitors: An in vitro and in silico approach toward antidiabetic drug design. *Archiv der Pharmazie* **2024**, *357* (8), 2400140.
(58) Zaib, S.; Ibrar, A.; Ramay, M.; Zahra, S.; Hökelek, T.; Simpson, J.; McAdam, C. J.; Awwad, N. S.; Ibrahium, H. A.; Frontera, A. Centroid··· centroid and hydrogen bond interactions as robust supramolecular units for crystal engineering: X-ray crystallographic, computational and urease inhibitory investigations of 1, 2, 4-triazolo [3, 4-a] phthalazines. *CrystEngComm* **2022**, *24* (29), 5324-5339.
(59) Rarey, M.; Kramer, B.; Lengauer, T.; Klebe, G. A fast flexible docking method using an incremental construction algorithm. *Journal of molecular biology* **1996**, *261* (3), 470-489.
(60) Release, S. 4: Desmond molecular dynamics system. *DE Shaw Research, New York, NY* **2017**.
(61) Lagunin, A.; Ivanov, S.; Rudik, A.; Filimonov, D.; Poroikov, V. DIGEP-Pred: web service for in silico prediction of drug-induced gene expression profiles based on structural formula. *Bioinformatics* **2013**, *29* (16), 2062-2063.
(62) Shakirova, R.; Orlova, N.; Elistratova, M.; Korobeynikova, A.; Mozyleva, Y.; Orlov, Y. Gene network analysis for complex disease using online bioinformatics tools. In *XXXVIII Symposium of Bioinformatics and Computer-Aided Drug Discovery*, 2022; pp 50-50.
(63) Harel, A.; Inger, A.; Stelzer, G.; Strichman-Almashanu, L.; Dalah, I.; Safran, M.; Lancet, D. GIFtS: annotation landscape analysis with GeneCards. *BMC bioinformatics* **2009**, *10* (1), 348.
(64) Jia, A.; Xu, L.; Wang, Y. Venn diagrams in bioinformatics. *Briefings in bioinformatics* **2021**, *22* (5), bbab108.
(65) Altermann, E.; Klaenhammer, T. R. PathwayVoyager: pathway mapping using the Kyoto Encyclopedia of Genes and Genomes (KEGG) database. *BMC genomics* **2005**, *6* (1), 60.
(66) Muley, V. Y. Functional Insights Through Gene Ontology, Disease Ontology, and KEGG Pathway Enrichment. In *Computational Virology*, Springer, 2025; pp 75-98.

(67) Grant, B. J.; Rodrigues, A. P.; ElSawy, K. M.; McCammon, J. A.; Caves, L. S. Bio3d: an R package for the comparative analysis of protein structures. *Bioinformatics* **2006**, *22* (21), 2695-2696. DOI: 10.1093/bioinformatics/btl461 From NLM.
(68) Kagami, L. P.; das Neves, G. M.; Timmers, L.; Caceres, R. A.; Eifler-Lima, V. L. Geo-Measures: A PyMOL plugin for protein structure ensembles analysis. *Comput Biol Chem* **2020**, *87*, 107322. DOI: 10.1016/j.compbiolchem.2020.107322 From NLM.
(69) Eruygur, N., Koçyiğit, U. M., Taslimi, P., Ataş, M. E. H. M. E. T., Tekin, M., & Gülçin, İ. (2019). Screening the in vitro antioxidant, antimicrobial, anticholinesterase, antidiabetic activities of endemic Achillea cucullata (Asteraceae) ethanol extract. *South African journal of botany*, *120*, 141-145.
(70) Taslimi, P., & Gulçin, İ. (2018). Antioxidant and anticholinergic properties of olivetol. *Journal of food biochemistry*, *42*(3), e12516.
(71) Gülçin, İ., Gören, A. C., Taslimi, P., Alwasel, S. H., Kılıc, O., & Bursal, E. (2020). Anticholinergic, antidiabetic and antioxidant activities of Anatolian pennyroyal (Mentha pulegium)-analysis of its polyphenol contents by LC-MS/MS. *Biocatalysis and agricultural biotechnology*, *23*, 101441.
(72) Öztaskın, N., Taslimi, P., Maraş, A., Gülcin, İ., & Göksu, S. (2017). Novel antioxidant bromophenols with acetylcholinesterase, butyrylcholinesterase and carbonic anhydrase inhibitory actions. *Bioorganic chemistry*, *74*, 104-114.
(73) Ishaq, M., Taslimi, P., Shafiq, Z., Khan, S., Salmas, R. E., Zangeneh, M. M., ... & Mohamad, H. (2020). Synthesis, bioactivity and binding energy calculations of novel 3-ethoxysalicylaldehyde based thiosemicarbazone derivatives. *Bioorganic chemistry*, *100*, 103924.
(74) Tokalı, F. S., Taslimi, P., Usanmaz, H., Karaman, M., & Şendil, K. (2021). Synthesis, characterization, biological activity and molecular docking studies of novel schiff bases derived from thiosemicarbazide: Biochemical and computational approach. *Journal of molecular Structure*, *1231*, 129666.
(75) Bursal, E., Aras, A., Kılıç, Ö., Taslimi, P., Gören, A. C., & Gülçin, İ. (2019). Phytochemical content, antioxidant activity, and enzyme inhibition effect of Salvia eriophora Boiss. & Kotschy against acetylcholinesterase, α-amylase, butyrylcholinesterase, and α-glycosidase enzymes. *Journal of food biochemistry*, *43*(3), e12776.
(76) Taslimi, P., Aslan, H. E., Demir, Y., Oztaskin, N., Maraş, A., Gulçin, İ., ... & Goksu, S. (2018). Diarilmetan compounds: discovery of potent aldose reductase, α-Amylase and α-Glycosidase inhibitors as new therapeutic approach in diabetes and functional hyperglycemia. *Int J Biol Macromol*, *119*, 857-863.